Immunity

Tcf1 and Lef1 cooperate with CTCF and Stat5 to critically regulate CD8+ T cell homeostasis

--Manuscript Draft--

Manuscript Number:	IMMUNITY-D-21-00919
Full Title:	Tcf1 and Lef1 cooperate with CTCF and Stat5 to critically regulate CD8+ T cell homeostasis
Article Type:	Research Article
Keywords:	T cell factor 1; CTCF; Stat5; CD8+ T cell homeostasis; homeostatic cytokines; genome architecture; transcriptome; chromatin accessibility; chromatin interaction hub; genomic architecture.
Corresponding Author:	Hai-Hui Xue Hackensack University Medical Center Nutley, NJ UNITED STATES
First Author:	Qiang Shan
Order of Authors:	Qiang Shan
	Shaoqi Zhu
	Xia Chen
	Xiang Li
	Weiqun Peng
	Hai-Hui Xue
Abstract:	CD8+ T-cell homeostasis is maintained by IL-7/IL-15 and Stat5 pathway. Here we show that deficiency in Tcf1 and Lef1 transcription factors impaired homeostatic proliferation of CD8+ T cells, by compromising IL-7/IL-15-induced activation of genes for cell cycle and DNA replication. Multiomics analyses demonstrated that Tcf1 recruited CTCF to the CD8+ T-cell genome, and that IL-7/IL-15 stimulation led to dynamic, Tcf1/Lef1-dependent CTCF binding changes. Hi-C coupled with network analyses revealed that Tcf1 and CTCF acted cooperatively to promote chromatin interactions and form highly connected, dynamic interaction hubs in naïve and proliferating CD8+ T cells. Furthermore, the Tcf1-CTCF cooperativity provided anchor points and proper chromatin configuration for docking phosphorylated Stat5 activated by IL-7/IL-15. Remarkably, ablating CTCF phenocopied proliferative defects observed in Tcf1/Lef1-deficient CD8+ T cells. These findings identified CTCF as a Tcf1 cofactor and uncovered an intricate interplay among Tcf1/Lef1, CTCF and Stat5 that modulates genomic architecture to guard CD8+ T-cell homeostasis.
Suggested Reviewers:	Ellen Rothenberg Caltech evroth@its.caltech.edu
	Keiji Zhao zhaok@nhlbi.nih.gov
	Cornelis Murre cmurre@ucsd.edu
Opposed Reviewers:	Ananda Goldrath direct competing research interests
	Fotini Gounari direct competing research interests
Additional Information:	
Question	**Response**

Standardized datasets<p>A list of datatypes considered standardized under Cell Press policy is available here. Does this manuscript report new standardized datasets?	Yes
Reviewers must have anonymous access to these standardized datasets that is free-of-cost. Please provide dataset locations and instructions for access here. If applicable, include accession numbers and reviewer tokens.<p>Please consult these Author's guides for more information: "Standardized datatypes, datatype-specific repositories, and general-purpose repositories recommended by Cell Press" and "How standardized datasets and original code accompany Cell Press manuscripts from submission through publication" or email us at immunity@cell.com. as follow-up to "Standardized datasets<p>A list of datatypes considered standardized under Cell Press policy is available here. Does this manuscript report new standardized datasets?"	https://www.ncbi.nlm.nih.gov/geo/query/acc.cgi?acc=GSE164713 Enter token snqtkeqwjlmpxub into the box
Original Code<p>Does this manuscript report original code?	Yes
Reviewers must have anonymous access to these original code that is free-of-cost. Please provide code location and instructions for access here.<p>Please consult this Author's guide for more information: "How standardized datasets and original code accompany Cell Press manuscripts from submission through publication" or email us at immunity@cell.com. as follow-up to "Original Code<p>Does this manuscript report original code?"	the code is in an open source repository https://github.com/lux563624348/HiC_Hubs

July 21st, 2021

Dr. Fabiola Rivas
Deputy Editor
Immunity

Dear Faby,

Enclosed please find our manuscript entitled "*Tcf1 and Lef1 cooperate with CTCF and Stat5 to critically regulate CD8⁺ T cell homeostasis*" by Shan and Zhu et al for your consideration of publication in *Immunity* as a Research Article. This is a co-submission with a manuscript entitled "*Lineage-determining transcription factor TCF-1 promotes chromatin intermingling between topologically associating domains in T cell progenitors*" by the Vahedi group at the UPenn.

The transcription factors Tcf1 and Lef1 have versatile functions in T cell development, anti-viral and anti-tumor immunity as we recently reviewed in *Nat. Rev. Immunol.* (https://doi.org/10.1038/s41577-021-00563-6). These factors contribute to organizing genomic architecture, but how this is mechanistically achieved remains a major knowledge gap. The two studies independently made the conceptual advance that Tcf1 and CTCF physically interact and have potent cooperativity in promoting chromatin looping and organizing topological configuration in 3D genome to regulate T cell maturation and functions.

Our study investigated how CD8⁺ T cell homeostasis is regulated, beyond the known γ_c cytokine-activated Stat5 pathway. We demonstrated that ablating Tcf1/Lef1 or CTCF showed a phenocopy in severely impairing homeostatic proliferation of mature CD8⁺ T cells. By employing multiomics approaches including in situ Hi-C and developing a novel algorithm named HiCHub, our study advanced our mechanistic understanding in the following aspects:

1. Tcf1 engages CTCF to organize CD8⁺ T cell genome. Tcf1 and CTCF show prevalent colocalization, and importantly, Tcf1/Lef1 are required for CTCF positioning in CD8⁺ T cell genome. Tcf1 and CTCF act cooperatively to form chromatin interaction hubs in CD8⁺ T cells in naïve state and during homeostatic proliferation.
2. CTCF is mobilized by homeostatic cytokines. Whereas 'constitutive' CTCF binding is associated with its insulator function, CTCF show dynamic changes in binding strength in response to homeostatic cytokines. The 'dynamic' CTCF cooperates with Tcf1 to induce chromatin contacts in support of cell cycle progression and DNA replication.
3. Tcf1 and CTCF provide anchor points for cytokine-activated Stat5. Stat5 is rapidly phosphorylated by homeostatic cytokines and translocated into the nucleus. Specific mapping of phosphorylated Stat5 occupancy reveals that Stat5 predominantly utilized CTCF- and/or Tcf1-bound genomic locations as anchor points during homeostatic proliferation, unlike antigen-activated CD8⁺ T cells where Stat5 access its own motifs.

The Tcf1-CTCF-Stat5 interplay in CD8⁺ T cells revealed by the mechanistic studies may have far-reaching impact on *in vitro* expansion of therapeutic immune cells such as CAR-T cells. Together with the co-submitted manuscript by the Vahedi group, these studies corroborate the notion that TCF-1 is a global genome organizer in T cells. These findings should be of broad interest to scientists in the fields of T cell biology, gene regulation in the immune system, and dynamic 3D genome organization in response to environmental cues. We would like to disseminate this new knowledge from the platform of *Immunity* and hope that you share the same enthusiasm.

Hackensack University Medical Center-Center for Discovery and Innovation |111 Ideation Way
Bldg. 102, Rm. A417, Nutley, NJ 07110 T: 201-880-3550 | Website: https://hmh-cdi.org/

For referees, we recommend Drs. Ellen Rothenberg (Caltech, evroth@its.caltech.edu), Keji Zhao (NHLBI/NIH, zhaok@nhlbi.nih.gov) and Cornelis Murre (UCSD, cmurre@ucsd.edu) for their expertise on higher-order genome organization in immune cells. We also respectfully request exclusion of Drs. Ananda Goldrath (UCSD) and Fotini Gounari (U of Chicago) from reviewing this work because of direct competing research interests.

All of the authors have approved this submission, certify that this work has not been reported previously and is not under consideration for publication elsewhere.

We have a related manuscript entitled "*Tcf1 and Lef1 orchestrate genomic architecture to supervise mature CD8⁺ T cell identity*", which is currently accepted in principle in *Nature Communications*. You may recall that this manuscript was previously submitted to *Immunity* in February, under the manuscript number "IMMUNITY-D-21-00137". That work laid the foundation for in-depth mechanistic investigation of Tcf1-CTCF cooperativity in regulating $CD8^+$ T cell homeostasis in this study.

Sincerely yours,

Hai-Hui Xue, MD & PhD
Member/Professor
Center for Discovery and Innovation
Hackensack University Medical Center

Weiqun Peng, PhD
Professor
Department of Physics
The George Washington University

Tcf1 and Lef1 cooperate with CTCF and Stat5 to critically regulate CD8$^+$ T cell homeostasis

Qiang Shan[1,5], Shaoqi Zhu[2,5], Xia Chen[1], Xiang Li[2],

Weiqun Peng[2,3], Hai-Hui Xue[1,3,4]

From [1]Center for Discovery and Innovation, Hackensack University Medical Center, Nutley, NJ 07110

[2]Department of Physics, The George Washington University, Washington DC, 20052

[4]New Jersey Veterans Affairs Health Care System, East Orange, NJ 07018

[5]These authors contributed equally to this work.

Running title: Tcf1, CTCF and Stat5 in CD8 homeostasis.

[3]Corresponding authors:

Hai-Hui Xue (ORCID: 0000-0002-9163-7669)

111 Ideation Way, Bldg. 102, Rm. A417, Nutley, NJ 07110

Tel: 201-880-3550; E-mail: haihui.xue@hmh-cdi.org

Weiqun Peng (ORCID: 0000-0001-5521-9091)

Science & Engineering Hall 4790, 800 22nd St NW, Washington, DC 20052

Tel: 202-994-0129; E-mail. wpeng@gwu.edu

CD8$^+$ T-cell homeostasis is maintained by IL-7/IL-15 and Stat5 pathway. Here we show that deficiency in Tcf1 and Lef1 transcription factors impaired homeostatic proliferation of CD8$^+$ T cells, by compromising IL-7/IL-15-induced activation of genes for cell cycle and DNA replication. Multiomics analyses demonstrated that Tcf1 recruited CTCF to the CD8$^+$ T-cell genome, and that IL-7/IL-15 stimulation led to dynamic, Tcf1/Lef1-dependent CTCF binding changes. Hi-C coupled with network analyses revealed that Tcf1 and CTCF acted cooperatively to promote chromatin interactions and form highly connected, dynamic interaction hubs in naïve and proliferating CD8$^+$ T cells. Furthermore, the Tcf1-CTCF cooperativity provided anchor points and proper chromatin configuration for docking phosphorylated Stat5 activated by IL-7/IL-15. Remarkably, ablating CTCF phenocopied proliferative defects observed in Tcf1/Lef1-deficient CD8$^+$ T cells. These findings identified CTCF as a Tcf1 cofactor and uncovered an intricate interplay among Tcf1/Lef1, CTCF and Stat5 that modulates genomic architecture to guard CD8$^+$ T-cell homeostasis.

$CD8^+$ T lymphocytes are cytotoxic cells that lyse cells infected with intracellular pathogens as well as malignantly transformed cells (McLane et al., 2019; Williams and Bevan, 2007). The naïve $CD8^+$ T cell pool must be maintained at or restored to a stable size after hematopoietic injuries caused by infections or cytoreductive chemotherapy and radiotherapy, so as to sustain immunocompetence (Velardi et al., 2021). It has been well established that the homeostasis of naïve $CD8^+$ T cells rely on signals derived from self-peptide-MHC complexes and cytokines in the common cytokine γ-chain (γ_c) family (Surh and Sprent, 2008; Takada and Jameson, 2009). Among γ_c cytokines, IL-7 and IL-15 have more dominant roles in promoting $CD8^+$ T cell survival and homeostatic proliferation (Berard et al., 2003; Schluns et al., 2000; Tan et al., 2001). IL-7 and IL-15 activate Jak1 and Jak3 kinases, which in turn phosphorylate Stat5a and Stat5b transcription factors (TFs), resulting in Stat5 dimerization and nuclear translocation (Leonard et al., 2019). In fact, deletion of both Stat5 TFs severely depletes mature $CD8^+$ T cells (Yao et al., 2006). In spite of the clearly mapped IL-7/15-Stat5 pathway that connects environmental input to nuclear TF activity, intrinsic determinants that control $CD8^+$ T cell homeostasis remain incompletely understood.

Tcf1 and Lef1 are Tcf/Lef family TFs that are abundantly expressed in T lineage cells, and have versatile functions in T cell development and mature T cell responses to pathogen challenges (Zhao et al., 2021). In $CD8^+$ lineage cells, Tcf1/Lef1 are critical for establishing $CD8^+$ T cell identity by suppressing $CD4^+$ lineage-associated genes during late stages of thymic development (Xing et al., 2016). In antigen-experienced $CD8^+$ T cells, Tcf1 is essential for formation and longevity of memory $CD8^+$ T cells generated in

response to acute infections (Jeannet et al., 2010; Zhou et al., 2010), and for self-renewal of stem-like exhausted $CD8^+$ T cells generated in the context of chronic viral infection (Im et al., 2016; Leong et al., 2016; Shan et al., 2021; Utzschneider et al., 2016). Tcf1/Lef1 contain a highly conserved high-mobility-group (HMG) DNA binding domain, and HMG proteins are known to cause DNA bending upon binding to the minor grooves of DNA double helix (Grosschedl et al., 1994). In fact, Lef1 binds to a minimal TCRα enhancer and causes a sharp DNA bending *in vitro* (Giese et al., 1995; Love et al., 1995). In a recent study, we investigated the postulated structural role of Tcf1/Lef1 in three dimensional (3D) genomic architecture, using multiomics approaches including Hi-C (Shan et al. in press). We found that Tcf1/Lef1 TFs modulated genomic organization on multiple scales including A/B compartments, topologically associated domains (TADs), and focal chromatin loops in mature $CD8^+$ T cells, and their structural functions provided constant supervision of $CD8^+$ T cell identity (Shan et al. in press). In spite of these advances, knowledge gaps remain on at least two major questions. The first is that Tcf1/Lef1-mediated DNA bending occurs at minor grooves of $\leq$10 bp resolution. Even if Tcf1 has close to 20,000 binding sites in naïve $CD8^+$ T cell genome, its broad impact on genomic structure cannot be solely explained by the DNA bending effects. Then what are the key partner(s) for Tcf1/Lef1 in regulating the genomic architecture and achieving T cell-specific genomic configuration? The second question is how Tcf1/Lef1's architectural roles contribute to regulation of T cell biology, beyond identity supervision. This is challenging because during infection-elicited $CD8^+$ T cell activation and differentiation process, Tcf1 and Lef1 are downregulated in fully differentiated effector $CD8^+$ T cells (Zhao et al., 2010). Tcf1 and Lef1 protein undergo rapid turnover as

demonstrated in human naïve $CD4^+$ T cells, with estimated half-life of 3.2 and 6.5 hrs, respectively (Wolf et al., 2020). It is therefore likely that Tcf1/Lef1-dependent structural changes in naïve $CD8^+$ T cells are erased or overwhelmed by extensive molecular rewiring because of rapid induction of Myc and activation of AP-1, NFAT and NF-κB family TFs downstream of T cell receptor (TCR) and costimulatory receptors (He et al., 2016; Philip et al., 2017).

In this study, we found that Tcf1 and Lef1 were intrinsically required for naïve $CD8^+$ T cell homeostasis, where their expression was sustained during homeostatic proliferation. Mechanistic analyses of multiomics data revealed CCCTC-binding factor (CTCF), a well-characterized architectural protein and a versatile transcription regulator (Ohlsson et al., 2001; Ong and Corces, 2014), as a novel regulatory co-factor of Tcf1. Tcf1 physically interacted with and recruited CTCF, and both factors exhibited prevalent cobinding on the $CD8^+$ T cell genome. The Tcf1/Lef1 and CTCF cooperativity not only promoted chromatin interaction and formation of highly connected, dynamic interaction hubs in naïve $CD8^+$ T cells, but also provided anchor points and proper chromatin configuration for docking of Stat5 activated by IL-7/15. Our findings revealed an intricate interplay among Tcf1/Lef1, CTCF and Stat5 that orchestrates genomic architecture to coordinately promote $CD8^+$ T cell homeostatic proliferation.

Results

Tcf1 and Lef1 are required for maintaining CD8$^+$ T cell homeostasis.

To bypass the requirements for Tcf1 and Lef1 in thymocyte development, we used hCD2-Cre transgene to ablate Tcf1 and Lef1 in mature T cells and the Rosa26-STOP-GFP (*Rosa26*^{GFP}) allele to mark Cre-active, target-deleted cells (Li et al., 2021), and effective deletion of both proteins was validated by intracellular staining (**Fig. S1A**). By enumerating GFP$^+$CD8$^+$ T cells in the spleens of hCD2-Cre$^+$*Rosa26*^{GFP}*Tcf7*$^{+/+}$*Lef1*$^{+/+}$ (WT) and hCD2-Cre$^+$*Rosa26*^{GFP}*Tcf7*$^{FL/FL}$*Lef1*$^{FL/FL}$ (dKO) mice, we found that WT and dKO CD8$^+$ T cells were detected at similar numbers in young mice of 6-12 weeks old (**Fig. 1A**). Whereas WT CD8$^+$ T cell numbers increased in older mice of 41-45 weeks old, dKO CD8$^+$ T cells showed numerical decrease in the older mice (**Fig. 1A**), suggesting that Tcf1/Lef1 deficiency compromised maintenance of CD8$^+$ T cell pool. To test this, we mixed WT or dKO CD45.2$^+$GFP$^+$CD8$^+$ T cells (as test cells) with WT CD45.1$^+$CD8$^+$ competitor cells at 1:1 ratio, and adoptively transferred into replete CD45.2$^+$ mice. When tracking at 1 week and 3 weeks post-transfer, whereas WT CD8$^+$ T cells persisted at a relatively stable level, dKO CD8$^+$ T cells exhibited substantial decline in the recipients (**Fig. 1B**). These observations indicate that Tcf1/Lef1-deficient CD8$^+$ T cells are less competitive in maintaining homeostasis.

Phenotypic analyses confirmed that dKO $CD8^+$ T cells were predominantly in $CD44^{lo}CD62L^+$ naïve state without aberrant activation (**Fig. S1B**), and were not detectably more prone to apoptosis than WT cells in aged mice (**Fig. S1C**). We hypothesized that Tcf1/Lef1 deficiency impaired homeostatic proliferation of $CD8^+$ T cells. To directly test this, we labeled mature $CD8^+$ T cells with cell-trace violet (CTV) and adoptively transferred those into lymphopenic *Rag1*$^{-/-}$ mice. While most of WT and *Lef1*$^{-/-}$ $CD8^+$ T cells underwent proliferation at 72 hrs post-transfer, fewer *Tcf7*$^{-/-}$ $CD8^+$ cells were dividing and the proliferative defect was further exacerbated in dKO $CD8^+$ cells (**Fig. 1C**). Similar results were obtained for WT and dKO $CD8^+$ cells when transferred into irradiated mice for 72 hrs (**Fig. 1D**). Importantly, Tcf1 expression was sustained in naïve WT $CD8^+$ T cells that underwent active cell division in lymphopenic environment (**Fig. 1E**), unlike differentiated effector $CD8^+$ T cells which downregulate Tcf1 expression (Zhao et al., 2010). These observations indicate an intrinsic requirement for Tcf1/Lef1 in $CD8^+$ T cell homeostasis.

Tcf1 and Lef1 regulate responsiveness of naïve $CD8^+$ T cells to homeostatic cytokines.

IL-7 and IL-15 both contribute to promoting homeostatic proliferation of $CD8^+$ T cells, with IL-7 having a stronger pro-survival effect and IL-15 showing a stronger pro-proliferative effect (Surh and Sprent, 2008). To facilitate mechanistic investigation, we used both cytokines in *ex vivo* culture to maintain naïve $CD8^+$ T cell viability and promote its proliferative response. WT and *Lef1*$^{-/-}$ $CD8^+$ T cells initiated cell division by

72 hrs of culture at similar rate and continued to proliferate *ex vivo*; on the other hand, *Tcf7*$^{-/-}$ and in particular dKO CD8^{+} cells were less responsive to IL-7/15 stimulation (**Fig. 2A**). Thus, *ex vivo* culture with IL-7/15 reproduced key features of homeostatic proliferation process *in vivo*. It is of note that dKO CD8^{+} cells were able to proliferate in response to TCR stimulation *in vitro*, albeit showing modestly delayed cell division (**Fig. S2A**). In addition, the expression of IL-7 and IL-15 receptor components, *i.e.*, γ_c, IL-2Rβ and IL-7Rα were not detectably altered in *Tcf7*$^{-/-}$, *Lef1*$^{-/-}$, or dKO CD8^{+} T cells compared with WT cells (**Fig. S2B**). Both IL-7 and IL-15 activate Stat5 and PI3K-Akt pathways (Leonard et al., 2019). The magnitude and kinetics of Stat5a phosphorylation at the Tyr694 and Akt phosphorylation at the Ser473 residues were similar between WT and dKO CD8^{+} T cells when stimulated with IL-7/15 in vitro (**Fig. S2C**). These data indicate that Tcf1/Lef1-deficiency does not compromise T cell proliferative capacity in general and does not compromise signaling pathways activated by homeostatic cytokines, and further suggest that Tcf1 and Lef1 critically regulate integration of IL-7/15-derived signals in the nucleus for promoting cell cycle progression.

The data above also demonstrated the functional redundancy between Tcf1 and Lef1 in regulating CD8^{+} T cell homeostasis, with Tcf1 showing a more dominant role. To unravel the Tcf1/Lef1-controlled molecular circuits that programmed CD8^{+} homeostatic proliferation, we focused on dKO CD8^{+} T cells for downstream molecular analyses. We first performed RNA-Seq on WT and dKO CD8^{+} T cells at naïve state and those after 72-hr stimulation with IL-7/15. This time point was selected because the cells were not all committed to cycling and remained responsive to the cytokine stimulation. PCA analysis

showed each group was in distinct clusters (**Fig. S3A**). By performing four critical pairwise comparisons (**Fig. S3B**) and requiring ≥2-fold expression changes and FDR<0.05 as key criteria using CuffDiff (Trapnell et al., 2013), 2,110 differentially expressed genes (DEGs) were identified and resolved into 7 distinct clusters by K-means clustering analysis (**Fig. 2B**). Genes in the Expression Cluster 1 (ExpC1) and ExpC2 exhibited increased expression in response to IL-7/15 stimulation, and functional annotation using the DAVID bioinformatics resources (Huang da et al., 2009) showed that these genes were associated with cell cycle, DNA replication, lipid metabolism and mitochondrion, consistent with the needs for cell proliferation (**Fig. 2C**). Whereas the expression of most genes in ExpC1 and ExpC2 were similar between WT and dKO $CD8^+$ T cells before stimulation, those in ExpC1 showed impaired induction in IL-7/15-stimulated dKO $CD8^+$ T cells (**Fig. 2B**). The ExpC1 genes were predominantly regulators of cell cycle and DNA replication, such as those encoding cyclins, cyclin-dependent kinases, Foxm1, Eomes, and E2F family TFs that are known to promote cell cycle progression (**Fig. 2D**). Other IL-7/15 induced genes in ExpC2 were not affected in stimulated dKO $CD8^+$ T cells (**Fig. 2B, 2C**), but the enrichment score and significance for "cell cycle" were substantially lower than those in ExpC1, suggesting that major aspects of cell cycle regulation were impaired by Tcf1/Lef1 deficiency.

On the other hand, ExpC6 and C7 genes were downregulated in WT $CD8^+$ T cells after stimulation and were enriched in functions including immune system process, and associated transcription factors, cytokines and cytokine receptors (**Fig. S3C, S3D**). Genes of interest in these clusters included early response TFs in the Egr and AP1 family,

IL-6 receptor chains, and interferon-induced genes such as *Mx1* and *Oas3* (ExpC7, **Fig. S3C, S3D**). These genes were also downregulated in IL-7/15-stimulated dKO $CD8^+$ T cells to similar levels as stimulated WT cells, although ExpC6 genes were already downregulated in naïve dKO cells. These observations suggest that $CD8^+$ T cells may tune down immune responses during homeostatic proliferation process. Our recent study focused on DEGs between WT and dKO $CD8^+$ T cells at the naïve state, which were captured in ExpC3-6 clusters herein. In naïve $CD8^+$ T cells, Tcf1/Lef1 provided constant supervision of $CD8^+$ T cell identity by 1) repressing lineage-inappropriate genes such as *Cd79b* in B cells, *Foxp3* and *Nrp1* in Treg cells, 2) restraining induction of genes associated with effector $CD8^+$ T cell program, such as *Prdm1*, *Fasl*, *Gzmb*, and *Ccl5* (Shan et al, in press), and these genes were in ExpC3 and C4. Tcf1/Lef1 also positively regulated key T cell identity genes such as *Myb* and *Ccr7*, which were in ExpC5 and C6, respectively. The expression pattern changes in naïve WT and dKO $CD8^+$ T cells in ExpC3-5 were largely preserved in IL-7/15-stimulated cells, albeit with some variations (**Fig. 2B**). In spite of their important functions in naïve cells, genes in ExpC3-5 were less responsive to IL-7/15 stimulation, and we therefore posit that their expression changes may not contribute significantly to the defective homeostatic proliferation observed in dKO $CD8^+$ T cells. In contrast, cell cycle regulator genes were mostly in ExpC1, where their expression was unaffected in dKO cells at naïve state but showed inadequate induction after IL-7/15 stimulation. These observations suggest an interesting possibility that Tcf1/Lef1 controlled a distinct set of genes and predetermined their ability to respond to homeostatic cytokines.

Chromatin accessibility mapping reveals cooperativity of Tcf1/Lef1 with Stat5 and CTCF.

To gain mechanistic insights into how Tcf1/Lef1 controlled responsiveness to homeostatic cytokines, we mapped global Tcf1 binding in naïve $CD8^+$ T cells using ChIP-Seq approach, which identified 19,042 high-confidence Tcf1 peaks by stringent criteria (MACS2, fourfold enrichment, $P < 10^{-5}$ and FDR < 0.05) (Shan et al. in press). By stratifying with expression clusters, Tcf1 peaks were found at promoters (defined as the +/– 1 kb region flanking the transcription start site, TSS) of ~47% of all DEGs, and in ~91% of the DEG gene bodies and/or +/– 50 kb distal regions. These binding events may have accounted for Tcf1-mediated direct regulation of genes in ExpC3-C6, but appeared to be inconsequential in ExpC1, C2 and C7 in naïve $CD8^+$ T cells (**Fig. 2B**). For ExpC1 genes that were differentially expressed only after IL-7/15 stimulation, we hypothesized that the binding of Tcf1 to these gene loci predetermined their ability of transcriptional activation in response to homeostatic cytokines.

Tcf1 is known to regulate chromatin accessibility (ChrAcc) in T lineage cells (Emmanuel et al., 2018; Johnson et al., 2018; Shan et al., 2020). To obtain in-depth mechanistic insights into Tcf1/Lef1-mediated gene regulation during homeostatic proliferation, we used DNase-Seq to profile ChrAcc in naïve WT and dKO $CD8^+$ T cells before and after IL-7/15 stimulation, and each cell type/state was in distinct clusters on PCA (**Fig. S4A**). A total of 36,380 ChrAcc sites were detected from all four cell types/states, and among these, 5,202 sites were identified as differential (Diff) ChrAcc

sites based on the four key pairwise comparisons (as in **Fig. S3B**). These Diff ChrAcc sites were resolvable to 6 distinct clusters using unsupervised K-means clustering (**Fig. S4B**), and notably, the Diff ChrAcc and DEG clusters showed concordant changes (**Fig. S4C**). To identify potential regulators in collaboration with or downstream of Tcf1/Lef1, we analyzed the collection of ChrAcc sites with the chromVAR algorithm, which integrates ChrAcc signal strength and motif underlying the ChrAcc sites with enhanced performance (Schep et al., 2017; Yoshida et al., 2019). The top four motifs ranked by ChromVAR were all from the Tcf/Lef family, and were highly enriched in WT over dKO $CD8^+$ T cells at either naïve state or after IL-7/15-stimulation (**Fig. 3A, 3B**), consistent with our experimental setup and known roles of Tcf1/Lef1 in establishing and/or maintaining ChrAcc in T cells (Emmanuel et al., 2018; Johnson et al., 2018; Shan et al., 2020). Another top-ranked motif was Stat5a and Stat5b, which were more enriched in cytokine-stimulated WT or dKO $CD8^+$ T cells than in naïve counterparts (**Fig. 3A, 3B**). This result lent strong support to the validity of this approach, as Stat5 TFs are known to act downstream of IL-7 and IL-15 in $CD8^+$ T cell homeostasis (Leonard et al., 2019; Lin and Leonard, 2019). Strikingly, the motifs of CTCF and its spermatocyte paralog CTCFL were also highly enriched in cytokine-stimulated cells than in naïve cells (**Fig. 3A, 3B**). These analyses suggest that Tcf1/Lef1 may directly engage CTCF and Stat5 proteins to regulate T cell biology including $CD8^+$ T cell homeostasis.

To discern the requirements for CTCF in $CD8^+$ T cell homeostasis, we used CUT&RUN to map CTCF occupancy in WT and dKO $CD8^+$ T cells, before and after IL-7/15 stimulation, and the CTCF occupancy profiles in each cell type/state were in distinct

clusters on PCA (**Fig. S5A**). A total of 39,574 CTCF binding peaks was detected from all four cell types/states, and motif analysis of CTCF peaks using HOMER (Heinz et al., 2010) in any cell types/states showed that the top three motifs were invariably the CTCF motif (**Fig. S5B**), validating the specificity of the CUT&RUN-mediated mapping of CTCF binding sites. Among these, 6,876 sites showed differential CTCF binding strength across the four cell types/states and were resolved into 7 distinct clusters using K-means clustering (**Fig. 3C**). The CTCF clusters and DEG clusters showed remarkably similar patterns (Compare **Fig. 3C** *versus* **2B**): 1) clusters 1 and 2 showed IL-7/15-induced CTCF binding and gene expression (where the induction in clusters 1 depended on Tcf1 and Lef1), while in clusters 6 and 7, IL-7/15 stimulation diminished both; 2) clusters 5 and 6 exhibited diminished CTCF binding and gene expression in dKO $CD8^+$ T cells, while in clusters 3 and 4, both were elevated in the absence of CTCF. Importantly, the dynamic changes in CTCF occupancy were concordant with the CTCF binding site-associated DEGs (**Fig. 3D**). These observations suggest a strong cooperativity between CTCF and Tcf1 in regulating $CD8^+$ T cell gene expression, at naïve state and during homeostatic proliferation.

Dynamic and constitutive CTCF binding have distinct Tcf1/Lef1 dependency and functions in naïve $CD8^+$ T cells.

The dynamic CTCF binding patterns suggest an intriguing possibility that Tcf1/Lef1 engage CTCF as a cofactor for target gene regulation. By examining global Tcf1 and CTCF binding peaks in naïve $CD8^+$ T cells, we found remarkable overlap,

with >60% of Tcf1 peaks colocalizing with CTCF peaks (**Fig. 3E**). In addition, ectopically expressed FLAG-tagged Tcf1 in 293T cells co-immunoprecipitated with endogenous CTCF protein (**Fig. 3F**), further validating the unexpected potential cooperativity between Tcf1 and CTCF.

Among the 10,064 $Tcf1^+CTCF^+$ co-bound sites, 4,335 sites (~43%) were found in gene promoters, while the reminder was in distal regulatory regions including gene body and intergenic sequences. The $Tcf1^+CTCF^+$ co-bound sites at the promoters were not enriched in CTCF motifs (**Fig. S5C**), showed similar CTCT binding strength, similar ChrAcc and H3K27ac profiles between naïve WT and dKO $CD8^+$ T cells (**Fig. S5D**). In contrast, the 5,875 distal $Tcf1^+CTCF^+$ co-bound sites had CTCF as the top enriched motif, followed by those in Ets, Runx and Tcf/Lef TF motifs (**Fig. 4A**). These observations are consistent with the notion that distal enhancers are more closely associated with cell type-specific gene regulation than promoters (Shlyueva et al., 2014). We therefore focused on CTCF binding events in distal regulatory regions. CTCF binds DNA directly, as evidenced by the motif analysis (**Fig. 4A**), and we thus differentiated $Tcf1^+CTCF^+$ co-bound and CTCF solo sites into CTCF-direct (motif+) and -indirect (motif–) subset based on the presence and absence of CTCF motif, respectively. The CTCF solo sites (regardless of motif+ or motif– status) and motif+ $Tcf1^+CTCF^+$ cobound sites showed relatively stable CTCF binding, ChrAcc and H3K27ac signals between naïve WT and dKO $CD8^+$ T cells (**Fig. 4B**, and **4C** bottom panel), indicating that direct CTCF binding to DNA elements was largely unaffected by Tcf1/Lef1 deficiency. In contrast, at the motif– $Tcf1^+CTCF^+$ cobound sites, Tcf1 and CTCF binding peaks showed

concordant changes in binding strength, with most of these sites exhibited a consistent tendency of diminished CTCF binding, reduced ChrAcc and reduced H3K27ac signal strength in naïve dKO compared with WT $CD8^+$ T cells (**Fig. 4C**, top panel). These findings suggest that a substantial portion of CTCF binding was mediated by indirect recruitment by Tcf1/Lef1, where CTCF cooperated with Tcf1/Lef1 to maintain ChrAcc and function as transcriptional enhancers in naïve $CD8^+$ T cells.

CTCF's most recognized function lies in regulation of 3D genomic architecture, by establishing insulation between TADs and promoting chromatin looping within TADs (Ohlsson et al., 2001; Ong and Corces, 2014). Therefore, we examined the insulating capacity of CTCF binding events in our system. We recently used in situ Hi-C to map chromatin interactions and defined TADs in naïve $CD8^+$ T cells (Shan et al. in press). CTCF solo sites were more enriched at the TAD boundaries, consistent with the structural role of CTCF (**Fig. 4D**, top), while $Tcf1^+CTCF^+$ co-bound sites were found more frequently found within TAD, suggestive of a regulatory function (**Fig. 4D**, bottom). CTCF-bound regions at the TAD boundaries function as insulators (Gong et al., 2018), and CTCF soles sites had the highest insulation index; in contrast, motif–$Tcf1^+CTCF^+$ co-bound sites showed the lowest insulation index (**Fig. 4E**). These analyses support the notion that CTCF functions as a Tcf1 cofactor in gene regulation, besides its known insulator function. In addition to the global trend, comparison CTCF binding strength between naïve WT and dKO $CD8^+$ T cells using edgeR (Huber et al., 2015) identified 2,316 WT- and 662 dKO-specific CTCF binding sites ($\geq$ 2 fold, FDR $\leq$ 0.05) in naïve $CD8^+$ T cells, respectively. Significantly, the $Tcf1^+CTCF^+$ co-bound sites were

highly enriched in WT-specific, but not in dKO-specific CTCF binding sites (**Fig. 4F**). We recently demonstrated that Tcf1/Lef1 are responsible for maintain ChrAcc at an 'open' state in naïve $CD8^+$ T cells (Shan et al. in press). Interestingly, the Tcf1/Lef1-dependent cobound CTCF binding sites were associated with approximately 50% of Tcf1/Lef1-dependent open ChrAcc sites (**Fig. 4G**). For example, a cluster of 6 Tcf1/Lef1-dependent open ChrAcc sites upstream of *Myb* was bound by both Tcf1 and CTCF in WT $CD8^+$ T cells, and CTCF binding to these sites was lost in dKO $CD8^+$ T cells (**Fig. S5E**). In addition, a Tcf1/Lef1-dependent *Prdm1* silencer, located at 24 kb upstream of its TSS (Shan et al, in press), was bound by CTCF in WT $CD8^+$ T cells, and the CTCF binding and ChrAcc at the silencer were both diminished in dKO $CD8^+$ T cells (**Fig. S5E**). These observations suggest that Tcf1/Lef1 recruited CTCF to key regulatory elements and cooperatively maintain their ChrAcc state and transcriptional enhancer/silencer activity, contributing to regulation of identity and function of naïve $CD8^+$ T cells.

CTCF is mobilized by homeostatic cytokines to promote $CD8^+$ T cell proliferation

Besides the Tcf1-CTCF cooperativity observed in naïve $CD8^+$ T cells, CTCF binding strength exhibited dynamic changes in response to homeostatic cytokines, as exemplified in CtcfC1 and CtcfC2 sites (**Fig. 3C**). Interestingly, the increase in CTCF binding intensity at CtcfC1 sites was dependent on Tcf1/Lef1, and 36% of these sites were $CTCF^+Tcf1^+$ cobound sites, whereas that at CtcfC2 sites did not require intact expression of Tcf1/Lef1 and only 18% showed co-occupancy with Tcf1 (**Fig. 3C**). These

observations suggest that Tcf1 and CTCF cooperate to regulate responsiveness to homeostatic cytokines. Analysis of CtcfC1 sites with the Genomic Regions Enrichment of Annotations Tool (GREAT) (McLean et al., 2010) revealed that these Tcf1/Lef1-dependent, cytokine-induced dynamic CTCF sites were associated with lymphocyte activation, differentiation, proliferation and adhesion (**Fig. 5A**). Furthermore, CtcfC1 sites can be linked to 294 genes in ExpC1 cluster, showing Tcf1/Lef1-dependent expression induction by homeostatic cytokines (**Fig. 2B**), and 58 of the 294 ExpC1 genes were associated with cell cycle and 19 were with DNA replication. For example, Tcf1 bound to an upstream region of *Ccne1* (site #2 in **Fig. 5B**), downstream regions of *E2f3* (**Fig. 5C**) and *E2f7* (site #2 in **Fig. 5C**), and these Tcf1-bound sites had weak CTCF binding signals in naïve $CD8^+$ T cells, but showed increased CTCF binding strength upon IL-7/15 stimulation in WT $CD8^+$ T cells, while the induction was compromised in stimulated dKO $CD8^+$ T cells. The same pattern was also observed in upstream regions of Eomes (sites #2 and # 3 in **Fig. 5D**) and *Tyms* (encoding thymidylate synthase that produces dTMP for DNA replication and repair, site #4 in **Fig. 5D**), upstream regions and intron of *Setbp1* (encoding SET binding protein 1, which has integrative transcription activation function by recruiting the SET1/KMT2A complex to AT-rich promoters (Piazza et al., 2018)), and a downstream region of *Pgam1* (encoding the phosphoglycerate mutase 1 enzyme in the glycolytic pathway) (**Fig. 5D**). Notably, several Tcf1-bound regions were $Tcf1^+CTCF^+$ cobound sites in naïve $CD8^+$ T cells where CTCF binding required intact expression of Tcf1/Lef1, and IL-7/15-induced CTCF binding at these regions remained compromised in stimulated dKO $CD8^+$ T cells, likely secondary to the existing defects in naïve dKO cells. Such sites were observed in *Ccne1*

intron (site#1 in **Fig. 5B**), a downstream region of *E2f7* (site#3 in **Fig. 5C**), and upstream regions of *Ccne2* (**Fig. 5B**), Eomes (site#4 in **Fig. 5D**) and *Tyms* (sites #2 and #3 in **Fig. 5D**). These example cases highlight the highly cooperative nature between Tcf1/Lef1 and CTCF in supporting $CD8^+$ homeostasis.

On the other hand, not all cytokine-induced dynamic CTCF binding events occurred at Tcf1-bound sites, as observed at upstream regions of *Ccnb1* (**Fig. 5B**), *Eomes* (site#3 in **Fig. 5D**) and *Tyms* (site#4 in **Fig. 5D**). This is in line with the ability of CTCF to bind DNA directly as a TF; however, the cytokine-induced CTCF solo sites remained dependent on Tcf1/Lef1, suggesting that Tcf1/Lef1 deficiency may have limited accessibility by CTCF due to chromatin topological changes (discussed below).

Tcf1 and CTCF cooperatively modulate chromatin interactions in response to homeostatic cytokines

CTCF has a well-established function in mediating chromatin looping (Ohlsson et al., 2001; Ong and Corces, 2014). We recently used Hi-C to demonstrate that Tcf1/Lef1 promote chromatin interactions on multiple scales in naïve $CD8^+$ T cells (Shan et al, in press). To investigate the Tcf1/Lef1-CTCF cooperativity in organizing genomic architecture in $CD8^+$ T cells undergoing homeostatic proliferation, we performed Hi-C on IL-7/15-stimulated WT and dKO $CD8^+$ T cells, each in two biological replicates. The Hi-C libraries were reproducible between the replicates (**Fig. S6A**), which were then pooled

for most downstream analyses to improve sensitivity. Similar to our previous study (Shan et al, in press), we analyzed chromatin interactions at a 10-kb resolution, and defined an interaction score for each 10-kb anchor by summing up its interaction with the rest of the chromosome in both directions. We then focused on the anchors that harbored the dynamic CTCF clusters (as defined in **Fig. 3C**), and determined the interaction scores for each dynamic CTCF site in all four cell type/states, *i.e.*, WT and dKO $CD8^+$ T cells at naïve state and after IL-7/15 stimulation. Most of the dynamic CTCF binding sites in each cluster showed concordant, statistically significantly changes in their interaction with neighboring chromatin regions (**Fig. 6A**). For example, CTCF binding sites in CtcfC5 and C6 showed Tcf1/Lef1-dependent reduction in CTCF binding strength and chromatin interaction in naïve dKO, compared with naïve WT $CD8^+$ T cells (**Fig. 6A**). The upstream regions of *Myb* and *Irf4* gene loci contained several Tcf1/Lef1-dependent CTCF binding sites in naïve $CD8^+$ T cells, and showed extensive interactions with *Myb* and *Irf4* TSS and flanking regions, observed as 'interaction patches', in naïve WT $CD8^+$ T cells (**Fig. S6B**). The interaction strength within the 'patches' was substantially diminished in naïve dKO $CD8^+$ T cells (**Fig. S6B**). On the other hand, in CtcfC1 and C2, CTCF showed increased binding strength in IL-7/15-stimulated WT compared with naïve WT $CD8^+$ T cells, and these sites exhibited increased chromatin interactions with neighboring regions in response to cytokine stimulation (**Fig. 6A**). For example, dynamic CtcfC1 sites were found at the TSS of *E2f3* and *Tnfsf8* genes, which encode E2F3 and CD30L, promote cell cycle progression and longevity of memory $CD8^+$ T cells (Nishimura et al., 2005), respectively. These sites showed induced chromatin interactions with neighboring regions harboring dynamic or constitutive CTCF sites, observed as

'interaction stripes', in IL-7/15-stimulated WT CD8$^+$ T cells (**Fig. S6C**). Importantly, the cytokine-induced CtcfC1-linked chromatin interaction was diminished in IL-7/15-stimulated dKO CD8$^+$ T cells (**Fig. 6A**), as observed in reduced interaction strength within the 'stripes' linked to *E2f3* and *Tnfsf8* TSSs in stimulated dKO CD8$^+$ T cells (**Fig. S6C**). These observations demonstrate strong cooperativity between Tcf1 and CTCF in promoting chromatin interactions in both naïve and homeostatic cytokine-stimulated CD8$^+$ T cells.

Whereas chromatin interactions are detected as 'stripes' connecting an anchor with neighboring regions or focal 'patches' connecting distal anchors, a more frequently observed form is broadly altered chromatin interactions within a TAD or sub-TAD (Madsen et al., 2020). To capture the highly interconnected nature, we devised a novel approach, dabbed as HiCHub, to assess chromatin interaction from a network perspective using the igraph platform. In this approach, we first extracted all interactions with the same directional changes between two cell types/states through pairwise comparisons, and then identified 3D chromatin interaction clusters based on connectivity among bins anchoring these interactions (**Fig. S6D**). The 3D clusters were then projected onto one-dimensional genomic regions, followed by integrative comparative analysis of numbers, strength and statistical significance of chromatin interactions among the regions. The analytical output is to generate cell type/state-specific, highly connected interaction hubs. We applied a refined version of HiCHub to comparative analysis between naïve WT and dKO CD8$^+$ T cell HiC data, and identified 390 naïve WT-specific and 688 naïve dKO-specific chromatin interaction hubs. As demonstrated above, this work revealed

Tcf1/Lef1-dependent CTCF recruitment and potent Tcf1-CTCF cooperativity in naïve WT $CD8^+$ T cells (**Fig. 4** and **6A**). Focused comparison CTCF CUT&RUN data between naïve WT and dKO $CD8^+$ T cells identified 2,316 naïve WT-specific CTCF peaks, which were more enriched in naïve WT-specific hubs (**Fig. 6B**, bars on left). For example, a WT-specific hub harboring the *Myb* gene showed strong connectivity of *Myb* with several naïve WT-specific CTCF peaks (**Fig. S6E**). Conversely, in the context of Tcf1/Lef1 deficiency, CTCF gained binding strength at 662 naïve dKO-specific sites, which were highly enriched in dKO-specific hubs (**Fig. 6B**, bars on right). A dKO-specific hub that harbors several *Ccl* genes showed extensive connectivity with the increased CTCF binding strength in dKO $CD8^+$ T cells (**Fig. S6E**). These findings further support Tcf1 and CTCF cooperativity is critical for promoting chromatin interactions and forming proper chromatin configuration and genomic architecture in $CD8^+$ T cells.

Applying the HiCHub approach to comparison between naïve WT and IL-7/15-stimulated WT $CD8^+$ T cell HiC data identified 1,482 naïve WT- and 478 stimulated WT-specific hubs. Focused comparison of CTCF CUT&RUN data between naïve and stimulated WT $CD8^+$ T cells identified 1,969 sites with increased CTCF binding strength in response to IL-7/15 stimulation, and these sites were highly enriched in stimulated WT-specific hubs (**Fig. 6C**, bars on right). These observations indicate a highly coordinated nature of dynamic CTCF binding and chromatin interaction changes in $CD8^+$ T cells responding to homeostatic cytokines. For example, the 'interaction patches' between the *Eomes* gene and its ~300 kb upstream CTCF clusters, and those among the *Setbp1* gene and multiple upstream CTCF clusters in the 200-500 kb range, showed

increased interaction strength in stimulated over naïve WT $CD8^+$ T cells (**Fig. 6D**). Each gene was found in stimulated WT-specific hubs as determined by the network analysis, where they showed high degree of connectivity with cytokine-induced dynamic CTCF peaks in the 3D space (**Fig. 6E**).

We next investigated if Tcf1/Lef1 contributed to cytokine-induced chromatin interactions in $CD8^+$ T cells undergoing homeostatic proliferation, beyond their demonstrated function in naïve $CD8^+$ T cells. The chromatin interaction strength in stimulated WT-specific hubs exhibited evident reduction in stimulated dKO $CD8^+$ T cells, whereas that in random regions was similar between stimulated WT and dKO $CD8^+$ T cells (**Fig. 6F**, two right columns). Significantly, the interaction strength in WT-specific hubs that were linked with dynamic CTCF peaks in the CtcfC1 cluster, but not those in the Ctcf2 cluster, showed more marked reduction in stimulated dKO $CD8^+$ T cells (**Fig. 6F**, two left columns). These comparisons suggest that Tcf1/Lef1-dependent CTCF mobilization was correlated with corresponding chromatin interaction changes. To further develop this notion, HiCHub was applied to comparison between stimulated WT and stimulated dKO $CD8^+$ HiC data, identifying 329 stimulated WT- and 1,039 stimulated dKO-specific hubs. The 1,054 CTCF peaks, which were specific to stimulated WT over stimulated dKO $CD8^+$ T cells, were more enriched in the stimulated WT-specific hubs (**Fig. 6G**, bars on left). The concordant reductions in CTCF binding and chromatin interaction strength in stimulated dKO cells were evidently observed at the *Eomes* and *Setbp1* loci (lower right diamond graphs in **Fig. 6D**). It is particularly noteworthy that these CtcfC1 peak-linked chromatin interactions were not detectably

different between naïve WT and dKO CD8$^+$ T cells (not depicted), and only became notably different after stimulation by homeostatic cytokines. These observations highlight a requirement for Tcf1 and Lef1 in organizing chromatin interaction changes in CD8$^+$ T cells undergoing homeostatic proliferation.

Stat5 cooperates with Tcf1/Lef1 and CTCF to promote CD8$^+$ T cell homeostasis.

IL-7/15-Stat5 pathway is the known central player in promoting homeostatic proliferation of CD8$^+$ T cells (Surh and Sprent, 2008). Given the newly revealed functions of Tcf1/Lef1 and CTCF in this critical process, we next investigated their interplay with Stat5. Upon IL-7/15 stimulation, Stat5a is rapidly phosphorylated (as seen in **Fig. S2C**) and translocates into the nuclei as dimers/tetramers for target gene regulation. The Stat5 signaling is intrinsically transient, because of several negative feedback mechanisms including activation of phosphatases and induction of Suppressor of Cytokine Signaling genes (Lin and Leonard, 2019). To capture early Stat5 binding before negative regulation takes effects, we cultured naïve WT CD8$^+$ T cells *ex vivo* with IL-7/15 for 0, 3 and 24 hrs and used pY694 Stat5a antibody to perform CUT&RUN. The use of anti-pY694 Stat5a instead of total Stat5 antibodies was expected to detect cytokine-activated new binding events with reduced background. Detection of pStat5 was made possible by treating the fixed cells with SDS to decondensate the chromatin and exposed the pY694 epitope which was otherwise buried within Stat5 dimers/tetramers. Indeed, while few binding events were detected at 0 hr, over 3,500 sites were newly occupied by pStat5 after 3-hr stimulation, and additional ~17,000 pStat5 binding sites

were detected in $CD8^+$ T cells after 24-hr stimulation (**Fig. S7A, S7B**). It is of note that although Stat5 was phosphorylated within minutes and the phosphorylation plateaued by one hour in naïve $CD8^+$ T cells (**Fig. S2C**), it took longer for pStat5 to reach and establish stable contact with its genomic target sites. GREAT analysis of pStat5 peaks at 24-hr showed strong association with cell cycle, DNA replication and cytokine production (**Fig. S7C**). Motif analysis of pStat5 peaks unexpected identified CTCF as the most enriched motif, followed by Ets, Spi1 and Runx motifs, while Stat5 motif ranked lower (**Fig. S7D**). This is in contrast to global mapping of Stat5a/b in IL-2-restimulated, activated $CD8^+$ T cells where Stat5 motif is top-ranked (Lin et al., 2012), and the difference is likely due to extensive transcriptomic and 3D genome structural changes between naïve and activated T cells (He et al., 2016; Philip et al., 2017). Comparative analysis further showed extensive colocalization of pStat5 with $Tcf1^+CTCF^+$ cobound sites, CTCF sole and Tcf1 solo binding sites (**Fig. 7A**). In addition, Stat5a in its native or constitutively active form (Stat5a-1*6 containing H299R and S711F mutation, (Onishi et al., 1998)) coimmunoprecipitated with CTCF as well as Tcf1 (**Fig. 7B**). These data suggest that in $CD8^+$ T cells undergoing homeostatic proliferation, Stat5 predominantly used CTCF and Tcf1 as anchor points, in addition to exploring its own motifs to gain access to target genes to promote cell cycle progression.

To further determine how pStat5a binding was affected by Tcf1/Lef1 deficiency, we performed pStat5a CUT&RUN on dKO $CD8^+$ T cells that were cocultured *ex vivo* with IL-7/15 for 24 hrs (**Fig. S7A**). Compared with WT cells, 1,116 pStat5 peaks showed decreased binding strength in IL-7/15-stimulated dKO $CD8^+$ T cells (**Fig. 7C**). These

stimulated WT-specific pStat5a binding sites were associated with T cell activation, proliferation, and differentiation, as determined by GREAT analysis (**Fig. 7A**), and were linked to 306 of the 602 genes in ExpC1 (**Fig. 2B**). Among these pStat5a-linked ExpC1 genes, 59 and 19 genes were associated with cell cycle and DNA replication, respectively, reminiscent of the association of CtcfC1 sites and ExpC1. The top two motifs of WT-specific pStat5a sites were CTCF and Tcf/Lef consensus sequence (**Fig. 7E**). In fact, nearly 80% of WT-specific pStat5a peaks were found at Tcf1- and/or CTCF-prebound sites (**Fig. 7F**). These observations further support the notion that homeostatic cytokine-induced Stat5 binding sites, especially the Tcf1/Lef1-dependent ones, utilized CTCF and Tcf1-occupied locations as anchor sites.

At most of the $Tcf1^{+}CTCF^{+}$ cobound sites, Tcf1/Lef1 deficiency diminished CTCF binding in naïve cells (**Fig. 4C**), which in turn compromised pStat5a recruitment after cytokine stimulation. Such $Tcf1^{+}CTCF^{+}$-dependent pStat5a binding sites were observed at site#3 downstream of *E2f7* (**Fig. 5C**), site#4 upstream of *Eomes* (**Fig. 5D**), site#2 upstream of *Wee1* (encoding a G2 checkpoint kinase), site#1 downstream of *Fbxo5* (encoding early mitotic inhibitor 1, Emi1, that regulates coupling of DNA replication with mitosis (Di Fiore and Pines, 2007)) (**Fig. S7E**). On the other hand, CTCF solo sites were mostly independent of Tcf1/Lef1 (**Fig. 4B**), and near 40% of WT-specific pStat5a sites colocalized with 'constitutive' CTCF binding sites in stimulated WT and dKO cells (group 2 in **Fig. 7G**). This observation suggests that CTCF solo sites served as anchors for pStat5a recruitment as well, as seen at site#1 downstream of *E2f7* (**Fig. 5C**), an upstream site for *E2f8*, and sites#2 and 3 downstream of *Fbxo5* (**Fig. S7E**). Given the

direct DNA binding capacity of Stat5 as a transcription factor, it is not surprising that WT-specific pStat5a bound to regions that were devoid of evident Tcf1 or CTCF peaks (group 3 in **Fig. 7G**), as observed at site#1 upstream of *Tyms* (**Fig. 5D**) and site#1 upstream of *Wee1* (**Fig. S7E**).

As demonstrated above, dynamic CTCF binding sites such as those in CtcfC1 cluster gained binding strength in response to cytokine stimulation (**Fig. 3C** and **Fig. 5**). About 35% of WT-specific pStat5a peaks showed concordant changes with CTCF binding strength between stimulated WT and dKO $CD8^+$ T cells (group 1 in **Fig. 7G**). As observed at site#2 downstream of *E2f7* (**Fig. 5C**) and sites#1 and 2 at the *Setbp1* (**Fig. 5D**), the Tcf1-bound sites became occupied by CTCF and pStat5 in cytokine-stimulated WT cells, but the recruitment of both factors were impaired in dKO $CD8^+$ T cells.

Our extensive molecular analyses suggest a critical requirement for CTCF in $CD8^+$ T cell homeostasis. To directly test this, we generated hCD2-Cre^+*Rosa26*^{GFP} *Ctcf*$^{FL/FL}$ (*Ctcf*$^{-/-}$) mice and validated that ablating CTCF did not detectably comprise Tcf1 or Lef1 expression in naïve $CD8^+$ T cells (**Fig. S1A**). We then transferred CTV-labeled naïve WT and *Ctcf*$^{-/-}$ $CD8^+$ T cells into *Rag1*$^{-/-}$ mice. A substantial portion of WT $CD8^+$ T cells divided at least one time after 72 hrs; in contrast, few *Ctcf*$^{-/-}$ $CD8^+$ T cells showed cell division (**Fig. 7H**), while both WT and *Ctcf*$^{-/-}$ cells showed similar capacity of survival *in vivo* (**Fig. 7I**). The defect of *Ctcf*$^{-/-}$ cells was a phenocopy of *Tcf7*$^{-/-}$*Lef1*$^{-/-}$ dKO $CD8^+$ cells in the same assay (compare with **Fig. 1C**). These data provide

functional validation that Tcf1/Lef1 and CTCF have essential and cooperative roles in supporting homeostatic proliferation of $CD8^+$ T cells.

Discussion

$CD8^+$ T cell homeostasis is actively maintained to ensure protective immunity. Homeostatic cytokines, including IL-7 and IL-15, and their downstream Stat5 TFs have a central role in this process. This study reveals an unexpected complexity in regulation of $CD8^+$ T cell homeostasis on multiple scales, which requires coordinated actions by Tcf1/Lef1 and CTCF in establishing genome architecture, dynamic redistribution of CTCF and ensuing modulation of chromatin interactions, which in turn provide anchor points for Stat5 activated by homeostatic cytokines.

Tcf1 engages CTCF to organize $CD8^+$ T cell genome. Tcf1 and Lef1 control many aspects of T cell functions including lineage decision, identity supervision, and context-dependent differentiation (Zhao et al., 2021). Tcf1 and Lef1 have uniquely extensive interactions with chromatin, functioning as a pioneer factor to gain access to heterochromatin (Johnson et al., 2018) or as a histone deacetylase to modify histone (Xing et al., 2016). Developing from the notion that Tcf1 and Lef1 bend DNA upon binding to the minor groove in the double helix (Giese et al., 1995; Love et al., 1995), our recent study demonstrated a structural role of these TFs in the 3D genome architecture in mature $CD8^+$ T cells in their naïve state (Shan et al., in press). In this context, Tcf1 and

Lef1 promote formation of transcriptionally active A compartments, TADs, and focal chromatin looping in $CD8^+$ T cells, and such structural roles have important bearings on maintaining $CD8^+$ T cell identity and keeping $CD8^+$ T cells at naïve state. How this deed is mechanistically achieved has been a challenge, because in spite of extensive binding of Tcf1/Lef1 to the genome, direct DNA bending at base-pair level cannot be solely responsible for their profound impact on large genomic structure such as compartments and TADs.

Tcf1/Lef1 are historically known as effector TFs downstream of Wnt signaling pathway that stabilizes and activates β-catenin (Staal et al., 2008; Xue and Zhao, 2012). It is currently recognized that weak but multivalent interactions among TFs and cofactors can form phase-separated condensates for coordinated regulation of gene expression (Banani et al., 2017; Hnisz et al., 2017). β-catenin uses its intrinsic disorganized regions to partition into the Mediator condensates (Zamudio et al., 2019). However, the involvement of β-catenin in T lineage cells has been largely excluded (Zhao et al., 2020). Through genome-wide survey of chromatin accessibility profiles during $CD8^+$ T cell homeostatic proliferation in this study, we found that over 50% of Tcf1 binding sites were co-occupied by CTCF. Although the cooperativity of CTCF with cell identity-defining TFs has been observed, such as with MyoD in muscle cells (Arzate-Mejia et al., 2018; Dall'Agnese et al., 2019), the level of Tcf1-CTCF overlap was markedly higher in $CD8^+$ T cells. Importantly, a substantial portion of CTCF binding events lacked CTCF motif and was dependent on the intact expression of Tcf1 and Lef1, indicating direct recruitment of CTCF by Tcf1/Lef1 through physical interaction. The Tcf1/Lef1-

dependent CTCF binding events in $CD8^+$ T cells were concordant with changes in chromatin interactions in both naïve and cytokine-stimulated $CD8^+$ T cells, as measured by interaction scores or connectivity within interaction hubs. This observation was well in line with the known function of CTCF in chromatin loop assembly and spatial organization-based gene regulation in immune cells (Pongubala and Murre, 2021). Therefore, the structural role of Tcf1 and Lef1 is at least partly mediated through engaging CTCF as a structural cofactor to provide identity supervision in naïve $CD8^+$ T cells. Moreover, in response to homeostatic cytokines, Tcf1/Lef1 recruit additional CTCF to further modulate chromatin interactions, in the forms of 'stripes', 'patches' and 'hubs', to support cell proliferation needs.

CTCF is mobilized by homeostatic cytokines. Similar to the situation in all other cell types, CTCF binds $CD8^+$ T cell genome directly through its own motif at over 50% CTCF binding sites. These $Motif^+$ CTCF binding events were frequently found at the TAD boundaries and were largely independent of Tcf1 and Lef1. These features of the 'constitutive' CTCF binding were consistent with the insulator function of CTCF. Within the TADs, however, CTCF has been shown to have more dynamic distribution, through interaction with cell identity-defining TFs or influenced by environmental cues such as metabolic changes (Chisolm et al., 2017; Hu et al., 2018; Qi et al., 2021). In $CD8^+$ T cells, CTCF exhibited extensive changes in binding strength in response to homeostatic cytokines, and the Tcf1/Lef1-dependent $Tcf1^+CTCF^+$ cobound sites were critical for sustaining chromatin accessibility and maintaining active enhancer state in naïve as well as homeostatic cytokine-stimulated $CD8^+$ T cells. These observations indicate that

Tcf1/Lef1 utilize CTCF as a transcriptional cofactor at the regulatory element level, in addition to their cooperativity in organizing genomic architecture.

In addition to Tcf1/Lef1-dependent recruitment, the dynamic redistribution of CTCF binding mobilized by homeostatic cytokines may take different forms. As a TF itself, CTCF retained the capacity to directly bind to its consensus DNA sequence, and this is supported by a strong enrichment of its own motif. In focused analysis of Tcf1/Lef1-dependent Stat5 binding sites, we observed that homeostatic cytokine-activated Stat5 was recruited to constitutive CTCF solo sites and dynamic $Tcf1^{+}CTCF^{+}$ cobound sites. Given the capacity of CTCF and Stat5 to physically interact, we postulate that the activated Stat5 may also partly account for CTCF mobilization. In fact, Stat5 promotes chromatin interactions in super enhancers at IL-2-induced genes in preactivated $CD4^{+}$ T cells, with potential CTCF involvement (Li et al., 2017). Our data thus suggest an extensive Tcf1-CTCF-Stat5 tripartite cooperativity in activating cell cycle progression and DNA replication during homeostatic proliferation of $CD8^{+}$ T cells.

Tcf1/Lef1 constraint CTCF distribution on genome. On a global scale, our analyses in naïve $CD8^{+}$ T cells demonstrate a predominant role of Tcf1 and Lef1 in promoting chromatin interactions on multiple scales. However, we also observed that Tcf1/Lef1-deficient $CD8^{+}$ T cells formed distinct intra-TAD chromatin interactions and hubs that were not observed in Tcf1/Lef1-sufficient WT cells. In addition, this type of new interactions and hubs were also found in Tcf1/Lef1-deficient $CD8^{+}$ T cells that were exposed to homeostatic cytokines. Initially we considered that Tcf1 and Lef1 might be

directly involved in restraining chromatin interactions at some gene loci, but were not sure how that could be mechanistically achieved. This study revealed physical interaction of Tcf1 and CTCF and extensive co-occupancy of both factors across the $CD8^+$ T cell genome, especially at the 'non-constitutive' CTCF binding sites. We postulate that the abundantly expressed Tcf1 and Lef1 in T cells may constitute an anchor for a pool of CTCF proteins that are free from their structural or insulator duties. In the absence of Tcf1 and Lef1, the 'free' CTCF proteins are released and thus gain access to other TFs; given the intrinsic capacity of CTCF in promoting chromatin looping, the 'freed' CTCF may contribute to the unusual genomic architectural changes in $CD8^+$ T cells lacking Tcf1 and Lef1. In support of this notion, we did observe highly concordant changes of CTCF binding events and associated interaction scores, as well as high degree of enriched CTCF binding in interaction hubs specific to Tcf1/Lef1-deficient $CD8^+$ T cells, in both naïve and cytokine-stimulated status.

Tcf1/Lef1 predetermine responsiveness to homeostatic cytokine. Like all other TFs, Tcf1 bound to many genomic locations in naïve $CD8^+$ T cells, but only a small fraction of Tcf1-assocation genes showed altered gene expression upon ablation of Tcf1 and Lef1. It has been a challenge to understand whether the transcriptionally inconsequential Tcf1 binding events contribute to T cell biology. Unlike profound Tcf1/Lef1 downregulation in TCR-stimulated, differentiating $CD8^+$ T cells, the expression of Tcf1/Lef1 proteins was preserved during $CD8^+$ T cell homeostatic proliferation, providing an important biological context to investigate the functional link of Tcf1 binding events. In this setting, over 600 genes that were not differentially expressed in Tcf1/Lef1-deficient $CD8^+$ T cells

in naïve state, showed insufficient induction after cytokine stimulation. Half of these genes were bound by Tcf1 at promoter regions, and a vast majority of these genes was associated with Tcf1 binding in distal regions flanking the loci. These Tcf1 binding events therefore were not immediately impactful in naïve $CD8^+$ T cells, but predetermined the ability of their associated genes to respond to stimulation by homeostatic cytokines. We hence propose the concept of 'pre-programming" of cytokine responsiveness by strategic Tcf1/Lef1 positioning in a $CD8^+$ T cell genome. At least two mechanisms can be considered for the Tcf1/Lef1-mediated 'pre-programming'. Firstly, Tcf1/Lef1-bound sites as anchors for cytokine-mobilized CTCF and Stat5 through direct recruitment or cooperative binding to composite DNA elements, where Tcf1/Lef1 are 'directly' involved. Secondly, through their structural roles in organizing 3D genomic architecture, Tcf1 and Lef1, together with CTCF, create a proper chromatin configuration with highly organized chromatin accessibility and interactions, which is permissible for Stat5 after activation. In this context, Tcf1/Lef1 do not need to be at the docking sites, and Stat5 proteins can access their motif elements directly or through interaction with TFs in other families such as Ets and Runx. This concept of 'TF-mediated pre-programming' might be broadly applicable to the responsiveness of T cells to stimulation of TCR, costimulatory or coinhibitory receptors.

In summary, our integrated multi-omics and functional analyses reveal an intrinsic requirement for Tcf1 and Lef1, and their cooperativity with CTCF, in maintaining $CD8^+$ T cell homeostasis. These data provide a direct connection of the well-established IL-7/15-Stat5 pathway with novel intrinsic regulators and a broad context of

3D genomic architecture. Our findings further suggest that the interplay of Tcf1/Lef1, CTCF and Stat5 proteins could be explored as a key regulatory model to promote *in vitro* expansion of therapeutic immune cells such as CAR-T cells.

Acknowledgements

We thank the University of Iowa Flow Cytometry Core facility (J. Fishbaugh, H. Vignes and G. Rasmussen) and the HMH-CDI Flow Cytometry Core facility (M. Poulus and W. Tsao) for cell sorting, and S. Xing for his contribution during the early phase of this study. This study is supported in-part by grants from the NIH (AI112579 to H.-H.X., AI121080 and AI139874 to H.-H.X and W. P.).

The authors declare no conflict of interests.

Author contributions

Q.S. and X.C. performed the experiments and analyzed the data. S. Z. analyzed all the high throughput sequencing data, with assistance from X. L.; W.P. and H.H.X. conceived the project, supervised the study, and wrote the paper.

Figure Legends

Figure 1. **Tcf1 and Lef1 are necessary for maintaining naive CD8$^+$ T cell homeostasis**.

A. Enumeration of splenic naive GFP$^+$CD8$^+$ T cells in WT and dKO mice at indicated age groups. Data are means ± s.d. from ≥3 experiments.

B. Competitive persistence of naïve CD8$^+$ T cells in replete hosts. CD45.2$^+$ WT or dKO GFP$^+$CD8$^+$ T cells (as test cells) were mixed with CD45.1$^+$ WT CD8$^+$ competitor cells at 1:1 ratio, and then adoptively transferred into replete CD45.2$^+$ mice. The test to competitor cell ratio was determined at 1 and 3 weeks after the transfer.

C. Homeostatic proliferation of naïve CD8$^+$ T cells in Rag-deficient, lymphopenic hosts. CD45.2$^+$GFP$^+$ CD8$^+$ T cells of indicated genotypes were labeled with cell-trace violet (CTV), transferred into *Rag1*$^{-/-}$ hosts and monitored for cell division as a function of CTV dilution after 72 hours. Representative histographs are from 3 experiments (left), and cumulative data on frequency of cells that underwent at least one division are means ± s.d.

D. Homeostatic proliferation of naïve CD8$^+$ T cells in irradiation-induced lymphopenic hosts. CTV-labeled WT or dKO CD45.2$^+$GFP$^+$ CD8$^+$ T cells were adoptively transferred into CD45.1$^+$ B6.SJL mice that were irradiated at 650 Rads, and CTV dilution was determined after 72 hrs. Representative histograms are from two independent experiments.

E. Detection of Tcf1 expression in naïve CD8$^+$ T cells undergoing homeostatic proliferation. CTV-labeled WT naive CD8$^+$ T cells were transferred into *Rag1*$^{-/-}$ hosts,

and 72 hrs later, and cells in Division 0-2 were intranuclearly stained for Tcf1. Half-stacked histograms are representative of 2 experiments, with values denote gMFI. Statistical significance for two group comparison was determined with Student's t-test, and that for multi-group comparison was first determined with one-way ANOVA, and Tukey's test was applied to indicated pair-wise comparison. *, $p<0.05$; **, $p<0.01$; ***, $p<0.001$; ns, not statistically significant. This annotation applies to all figures in this work unless specified otherwise.

Figure 2. **Tcf1 and Lef1 determine the ability of naive CD8$^+$ T cells to respond to homeostatic cytokines**.

A. Tracking cell division in culture *ex vivo*. Naïve GFP$^+$CD8$^+$ T cells of indicated genotypes were labeled with cell-trace violet (CTV), cultured in the presence of IL-7 and IL-15 for 72 (top) and 96 hrs (bottom), and monitored for cell division as a function of CTV dilution. Representative histographs are from 3 experiments (left), and cumulative data on frequency of cells that underwent at least one division are means ± s.d.

B. Defining expression clusters. RNA-Seq was performed on naïve WT or dKO GFP$^+$CD8$^+$ T cells, before and after 72-hr stimulation with IL-7 and IL-15, and DEGs were fractionated into 7 distinct expression clusters by K-means clustering analysis. Values in parentheses denote gene numbers in each cluster. In far right, red lines denote presence of high confidence Tcf1 binding peak(s) at corresponding gene promoters.

C. Gene ontology (GO) terms for genes in DEG clusters 1 and 2 as determined by the DAVID Bioinformatics Resources, with dot size denoting gene counts and dot color denoting statistical significance.

d. Heatmap showing the expression of select genes in cell cycle regulation from ExpC1.

Figure 3. CTCF cooperates with Tcf1/Lef1 in CD8$^+$ T cells and exhibits dynamic binding patterns during homeostatic proliferation.

A–B. ChrAcc-based prediction of top regulatory factors. DNase-Seq was performed on all four cell types/states, and the resulting ChrAcc sites were analyzed for motif enrichment using chromVAR. **A**. Rank-sorted TFs were plotted against motif variability on ChrAcc strength, and top-ranked TFs are marked. **B**. Heatmap showing 'accessibility score' of top-ranked motifs in different cell types/states, where each column represents a DNase-Seq library with replicates grouped together.

C. Defining dynamic CTCF binding clusters. CTCF CUT&RUN was performed on naïve WT or dKO GFP$^+$CD8$^+$ T cells, before and after 72-hr stimulation with IL-7 and IL-15. CTCF peaks with differential binding strength were fractionated into 7 distinct expression clusters by K-means clustering analysis. Values in parentheses denote CTCF peak numbers in each cluster. In far right, red lines denote presence of high confidence Tcf1 binding peak(s) at corresponding CTCF binding sites.

D. Correlation of CTCF dynamics with gene expression changes. Genes in expression clusters were stratified against genes linked to Diff. CTCF clusters, and the number of overlapping genes was counted. The value of each element in the correlation matrix is the ratio of the observed over expected overlapping gene counts, and all elements are color-coded based on the enrichment values.

E. Venn diagram showing overlap between high-confidence Tcf1 and CTCF binding sites in naïve WT CD8$^+$ T cells.

F. Tcf1 coimmunoprecipitates with CTCF. FLAG-tagged Tcf1 expression plasmid was transfected into 293T cells. The cell lysates were immunoprecipitated with anti-CTCF or control IgG followed by immunoblotting with anti-FLAG (left), or immunoprecipitated with anti-FLAG followed by immunoblotting with anti-CTCF (right). Shown are representative blots from 2-3 independent experiments.

Figure 4. Tcf1$^+$CTCF$^+$ cobound and CTCF solo sites have distinct features in naïve CD8$^+$ T cells.

A. Motif analysis of Tcf1$^+$CTCF$^+$ cobound sites at distal regulatory regions using HOMER. The top enriched motifs are listed together with motif logos, statistical significance and frequency of occurrence.

B–C. Heatmaps showing local chromatin characteristics of Tcf1$^-$CTCF$^+$ solo sites (**B**) and Tcf1$^+$CTCF$^+$ cobound sites (**C**) in distal regulatory regions in naïve CD8$^+$ T cells. Each type of sites was further stratified by the presence (Motif+) or absence (Motif–) of CTCF motifs.

D. The positional distribution of Tcf1$^-$CTCF$^+$ solo (top) and Tcf1$^+$CTCF$^+$ cobound (bottom) sites within TADs.

E. Profiles of insulation index around the four types of CTCF binding sites, where the index values are indicative of insulation effects.

F. Distribution of Tcf1$^+$CTCF$^+$ co-bound and CTCF solo sites within naïve WT- and dKO-specific CTCF-occupied locations.

G. Association of Tcf1/Lef1-dependent Tcf1$^+$CTCF$^+$ cobound sites (a total of 1,455 sites as defined in **F**) with naïve WT- and dKO-specific ChrAcc sites. The statistical significance in **F** and **G** was determined using the one-sided binomial test.

Figure 5. CTCF and pStat5a are mobilized by homeostatic cytokines.

A. GO terms for genes linked to CtcfC1 sites using GREAT, with dot size denoting term enrichment and dot color denoting statistical significance.

B–D. Tcf1 ChIP-Seq, CTCF and pStat5a CUT&RUN tracks at select gene loci encoding cyclins (**B**), E2F family TFs (**C**), and other cell cycle/DNA replication regulatory factors (**D**). Tcf1 ChIP-Seq was performed on naïve WT CD8$^+$ T cells (top track), CTCF CUT&RUN was performed on WT and dKO CD8$^+$ T cells before or after 72-hr IL-7/15 stimulation (middle 4 tracks), and pStat5a CUT&RUN was performed on WT and dKO CD8$^+$ T cells after 24-hr IL-7/15 stimulation (bottom 2 tracks). Whole or partial gene structure, transcription orientation and genomic scales are displayed on top of each panel. Cyan bars denote dynamic CTCF binding sites in the CtcfC1 cluster where CTCF binding strength was similar between naïve WT and dKO CD8$^+$ T cells. Orange bars mark CTCF binding sites where CTCF showed diminished binding strength in both naïve and stimulated dKO CD8$^+$ T cells. Bars with green edges mark WT-specific pStat5a binding sites.

Figure 6. Tcf1/Lef1 and CTCF cooperate to dynamically organize CD8$^+$ genomic architecture in response to homeostatic cytokines.

A. Concordant changes between CTCF binding strength and chromatin interaction anchored at the CTCF sites. The distribution of z-score-transformed CTCF binding strength in each of the seven dynamic CTCF clusters, as defined in **Figure 3C**, was plotted for all four cell types/states (top panels). The distribution of z-score-transformed interaction score of a CTCF-bound anchor was plotted for each CTCF cluster in all four cell types/states (bottom panels). *, $p<0.05$; **, $p<1e{-}10$; ***, $p<1e{-}30$ by one-sided MWU test. n-WT and n-dKO denote naïve WT and dKO $CD8^+$ T cells, respectively, and s-WT and s-dKO denote IL-7/15-stimulated WT and dKO $CD8^+$ T cells, respectively.

B, C, and **G**. Cell type/state-specific hubs are enriched with dynamic CTCF sites specific to the same state. **B**, comparison of naïve WT and dKO $CD8^+$ T cells; **C**, comparison of naïve WT and IL-7/15-stimulated WT $CD8^+$ T cells; and **G**, comparison of IL-7/15-stimulated WT and dKO $CD8^+$ T cells. Cell type/state-specific CTCF peaks were determined by comparing CTCF binding strength between the two cell types using edgeR, and cell type-specific interaction hubs were determined by comparing chromatin interaction strength and connectivity between the two cell types using HiCHub. Enrichment score is the ratio of observed to expected cell type-specific CTCF peaks on cell type-specific interaction hubs. The expected CTCF peak numbers were calculated by multiplying the total cell type-specific peak numbers with the ratio of total length of cell type/state-specific hubs to genome length. The statistical significance was determined using one-sided binomial test.

D. Tcf1/Lef1 deficiency impairs homeostatic cytokine-induced chromatin interactions. Diamond graphs of distance-normalized interactions from WashU Epigenome Browser at the *Eomes* and *Setbp1* gene loci are shown for naïve WT and IL-7/15-stimulated WT (top

panels) and stimulated dKO CD8$^+$ T cells (bottom panel). Blue boxes highlight chromatin interaction 'patches' showing marked induction in IL-7/15-stimulated WT CD8$^+$ T cells, but impaired induction in stimulated dKO cells. Shown in the bottom left panel are gene structures, Tcf1 ChIP-seq tracks in WT CD8$^+$ T cells, CTCF CUT&RUN tracks in all four cell types/states, along with genomic scale. Yellow bars mark dynamic CTCF binding sites, while green bars mark constitutive CTCF sites. *Note that diamond graphs are not shown for naïve dKO CD8$^+$ T cells, which did not show evident differences from naïve WT cells*.

E. Visualization of chromatin interaction hubs and connectivity with CTCF binding sites in IL-7/15-stimulated CD8$^+$ T cells. Comparing chromatin interactions in IL-7/15-stimulated and naïve WT CD8$^+$ T cells using HiCHub identified cell state-specific interaction hubs. Shown are stimulated WT-specific hubs containing the *Eomes* and *Setbp1* gene loci. In the hub network, grey lines denote increased chromatin interactions in IL-7/15-stimulated over naive WT CD8$^+$ T cells that were connected to gene promoters of interest (up to depth 3 nearest neighbors), and the nodes represent 10-kb bins. Circles denote bins containing gene promoters (with select gene symbols marked), and diamonds denote the presence of Tcf1 binding peaks. Triangles filled with red denote statistically significant increase in CTCF binding strength in IL-7/15-stimulated WT CD8$^+$ T cells.

F. Tcf1/Lef1 deficiency impairs homeostatic cytokine-induced chromatin interactions within hubs. Stimulated WT-specific interaction hubs were identified through comparison with naïve CD8$^+$ T cells, and interaction strength within all these 1,532 hubs, or hubs harboring dynamic CTCF binding sites in the CtcfC1 and CtcfC2 clusters were compared

between IL-7/15-stimulated dKO and WT dKO $CD8^+$ T cells. The distribution of Log2 fold changes (FC) in interaction strength were summarized in boxplots. As a negative control, 500 random regions with 20-bin length were used. The statistical significance was determined using one-sided MWU test.

Figure 7. Stat5 cooperates with Tcf1/Lef1 and CTCF to promote $CD8^+$ T cell homeostasis.

A. Venn diagram showing the overlap of pStat5 binding peaks in 24-hr IL-7/15-stimulated WT $CD8^+$ T cells with Tcf1 and CTCF peaks identified in naïve WT $CD8^+$ T cells.

B. Stat5a, in its WT or constitutively active form, coimmunoprecipitates with CTCF or Tcf1. Plasmids expressing WT Stat5a or constitutively active Stat5a-1*6, together with that expressing FLAG-tagged Tcf1 (in the right panel), was transfected into 293T cells. The cell lysates were immunoprecipitated with IgG or anti-CTCF (left) or anti-FLAG (right) followed by immunoblotting with anti-Stat5a. Data are representative from 2 experiments.

C. Heatmap showing differential pStat5a binding sites between WT and dKO $CD8^+$ T cells after 24-hr stimulation with IL-7/15.

D. GO terms for genes linked to stimulated WT-specific pStat5a peaks using GREAT, with dot size denoting term enrichment and dot color denoting statistical significance.

E. Top motifs of stimulated WT-specific pStat5a peaks using HOMER.

F. Pie chart showing overlap of stimulated WT-specific pStat5a peaks with Tcf1 and CTCF binding sites detected in naïve WT $CD8^+$ T cells.

G. Heatmaps showing distinct groups of stimulated WT-specific pStat5a peaks based on overlap with 1) dynamic CTCF with Tcf1 co-occupancy, 2) constitutive CTCF with no or weak Tcf1 cobinding, and 3) lack of strong CTCF or Tcf1 binding.

H–I. CTCF deficiency impairs homeostatic proliferation but not survival of $CD8^+$ T cells. WT or CTCF-deficient $CD45.2^+GFP^+$ $CD8^+$ T cells were labeled with CTV, transferred into *Rag1*$^{-/-}$ hosts, and monitored for cell division (**H**) and survival (**I**) after 72 hours. In **H**, representative histographs showing CTV dilution are from 2 experiments (top), and cumulative data on frequency of cells that underwent at least one division are means ± s.d. Shown in **I** are cumulative data on frequency of $7\text{-}AAD^+AnnexinV^+$ cells.

Legends to Supplemental Figures

Figure S1 (related to Figure 1). Tcf1/Lef1-deficient CD8$^+$ T cells remain in naïve state and are not prone to apoptosis.

A. Detection of Tcf1 and Lef1 expression. Splenic naïve CD8$^+$ T cells were isolated from mice of indicated genotypes and intranuclearly stained for Tcf1 and Lef1. Values denote geometric mean fluorescent intensity (gMFI). Data are representative from ≥2 experiments.

B. Detection of naïve CD8$^+$ T cells. Splenocytes were collected from mice of indicated genotypes, and TCRβ$^+$GFP$^+$CD8$^+$ T cells were analyzed for frequency of CD44^{lo}CD62L$^+$ naïve cells. Representative contour plots (left) are from 4 independent experiments, and cumulative data are means ± s.d.

C. Detection of apoptotic CD8$^+$ T cells. Splenic TCRβ$^+$GFP$^+$CD8$^+$ T cells were isolated from 22-27 week-old mice, and were analyzed for Annexin V and 7-AAD positivity. Representative contour plots (left) are from two independent experiments, and cumulative data on frequency of Annexin V$^+$ cells means ± s.d. ns, not statistically significant.

Figure S2 (related to Figure 2). Tcf1/Lef1 deficiency does not affect T cell proliferation and signaling in general.

A. T cell proliferation in response to TCR stimulation. GFP$^+$CD8$^+$ T cells of indicated genotypes were labeled with cell-trace violet (CTV), stimulated with plate-bound anti-CD3 in the presence of soluble anti-CD28 and IL-2 for 72 hrs (top) and 96 hrs (bottom), and monitored for cell division as a function of CTV dilution. Representative histographs are from 3 experiments (left), and cumulative data on frequency of cells that underwent at least one division are means ± s.d.

B. Detection of indicated cytokine receptor expression on GFP$^+$CD8$^+$ T cells. Representative half-stacked histographs are from 3 experiments (top), with values denoting gMFI. Cumulative data on gMFI (bottom) are means ± s.d, with no statistically significant differences observed and thus unmarked.

C. Detection of Stat5a and Akt phosphorylation in naïve CD8$^+$ T cells in response to homeostatic cytokines. CD45.2$^+$ WT and dKO GFP$^+$CD8$^+$ T cells were sort-purified and stimulated with IL-7 and IL-15 for indicated duration, and then immunoblotted with indicated antibodies. Gel images are representative from two independent experiments. The signal strength of pY694-Stat5a and pS473-Akt was normalized to respective total protein, and their time-dependent changes were plotted in the right panels. *Note that the pY694-Stat5a antibody also detects Tyr699-phosphorylated Stat5b*.

Figure S3 (related to Figure 2). Transcriptomic analyses of WT and Tcf1/Lef1-deficient CD8$^+$ T cells before and after IL-7/15 stimulation.

A. Principal component analysis (PCA) of RNA-Seq libraries. RNA-Seq was performed on naïve WT or dKO GFP^+CD8^+ T cells, before and after 72-hr stimulation with IL-7 and IL-15, each in three replicates.

B. Diagram showing key pair-wise comparisons to define the dynamic transcriptome.

C–**D**. Gene ontology analysis of homeostatic cytokine-repressed genes in ExpC6 (**C**) and ExpC7 (**D**), as determined by the DAVID Bioinformatics Resources. Dot size denotes gene counts, and dot color denotes statistical significance. Selected IL-7/15-repressed genes are shown in heatmaps (right panels).

Figure S4 (related to Figure 3). Analyses of ChrAcc in WT and Tcf1/Lef1-deficient $CD8^+$ T cells before and after IL-7/15 stimulation.

A. PCA of DNase-Seq libraries. DNase-Seq was performed on naïve WT or dKO GFP^+CD8^+ T cells, before and after 72-hr stimulation with IL-7 and IL-15, each in two to three replicates.

B. Defining ChrAcc clusters. Differential ChrAcc sites were identified based on the key comparisons as in **Fig. S3B**, and the dynamic ChrAcc sites were fractionated into 6 distinct expression clusters by K-means clustering analysis. Values in parentheses denote site numbers in each cluster. In far right, red lines denote presence of high confidence Tcf1 binding peak(s) at corresponding gene promoters. K-means clustering of.

C. Correlation between transcriptome and ChrAcc changes. Genes in expression clusters were stratified against genes linked to Diff. ChrAcc clusters, and the number of overlapping genes was counted. The value of each element in the correlation matrix is the ratio of the observed over expected overlapping gene counts, and all elements are color-coded based on the enrichment values.

Figure S5 (related to Figures 3 and 4). Features of CTCF binding sites in naïve $CD8^+$ T cells.

A. PCA of CTCF CUT&RUN libraries. CTCF CUT&RUN was performed on naïve WT or dKO GFP^+ $CD8^+$ T cells, before and after 72-hr stimulation with IL-7 and IL-15, each in two replicates.

B. Top motifs of CTCF binding peaks in naïve WT $CD8^+$ T cells as determined with HOMER. The top three most enriched motifs are listed together with motif logo and statistical significance.

C. Top motifs of $Tcf1^+CTCF^+$ cobound sites at gene promoters as determined with HOMER.

D. Heatmap showing local chromatin characteristics of $Tcf1^+CTCF^+$ cobound sites at promoters. For clarity, the Tcf1 peak signals were rescaled with a factor of 0.75, ChrAcc signals were rescaled with a factor of 2, and the H3K27ac signals were normalized by promoter read count in each library per million.

E. Distal Tcf1$^+$CTCF$^+$ cobound sites with concordant decrease in CTCF binding strength and ChrAcc in naïve dKO compared with WT CD8$^+$ T cells, as display at the *Myb* (left) and *Prdm1* (right) loci. Shown are Tcf1 ChIP-seq tracks in WT CD8$^+$ T cells (top), CTCF CUT&RUN tracks in WT and dKO CD8$^+$ T cells (middle), and DNase-Seq tracks in WT and dKO CD8$^+$ T cells (bottom). Whole or partial gene structure, transcription orientation, and genomic scale are displayed on top of each panel. Yellow boxes denote Tcf1$^+$CTCF$^+$ cobound site(s).

Figure S6 (related to Figure 6). Global analysis of chromatin interaction scores reveals Tcf1-CTCF cooperativity in organizing genomic architecture in CD8$^+$ T cells.

A. Scatterplots showing reproducibility of two biological replicates of Hi-C libraries from WT or dKO CD8$^+$ T cells that were stimulated with IL-7/15 for 72 hrs *ex vivo*. The *x*- and *y*-axis values for each data point (marked with a dot) represent the interaction scores of an anchor in replicate 1 (Rep1) and replicate 1 (Rep 2), respectively. The R values denote Pearson correlation coefficient.

B. Tcf1/Lef1 deficiency impairs chromatin interaction in naïve CD8$^+$ T cells. Diamond graphs were extracted from WashU epigenome browser, showing distance-normalized chromatin interactions in naïve WT (top) and dKO CD8$^+$ T cells (bottom) at the *Myb* (left) and *Irf4* (right) gene loci. Blue boxes denote chromatin interaction 'patches' showing marked reduction in dKO compared with WT CD8$^+$ T cells. Shown in the middle are gene structures, Tcf1 ChIP-seq tracks in WT CD8$^+$ T cells, CTCF CUT&RUN tracks in naïve WT and dKO CD8$^+$ T cells, along with genomic scale. Highlighted in yellow are Tcf1/Lef1-dependent CTCF binding sites.

C. Tcf1/Lef1 deficiency impairs homeostatic cytokine-induced chromatin interactions. Diamond graphs at the *E2f3* and *Tnfsf8* gene loci are shown for naïve WT and IL-7/15-stimulated WT (top panels) and stimulated dKO CD8$^+$ T cells (bottom panel). Blue boxes highlight chromatin interaction 'stripes' showing marked induction in IL-7/15-stimulated WT CD8$^+$ T cells, but impaired induction in stimulated dKO cells. Shown in the bottom left panel are gene structures, Tcf1 ChIP-seq tracks in WT CD8$^+$ T cells, CTCF CUT&RUN tracks in all four cell types/states, along with genomic scale. Yellow bars mark dynamic CTCF binding sites, while green bars mark constitutive CTCF sites. *Note that diamond graphs are not shown for naïve dKO CD8$^+$ T cells, which did not show evident differences from naïve WT cells*.

D. Diagram showing the workflow of identifying cell type/state-specific chromatin interaction (Chr. Int.) hubs and hub-associated target genes.

E. Visualization of chromatin interaction hubs and connectivity with CTCF binding sites in naïve CD8$^+$ T cells. Comparing chromatin interactions in naïve WT and dKO CD8$^+$ T cells using HiCHub identified cell type-specific interaction hubs. Shown on top is a WT-specific hub containing the *Myb* locus, where the nodes represent 10-kb bins and the lines represent chromatin interactions decreased in dKO CD8$^+$ T cells. At the bottom is a dKO-specific hub containing multiple *Ccl* genes, where the lines represent chromatin interactions increased in dKO CD8$^+$ T cells. Circles denote bins containing gene promoters (with select gene symbols marked), and diamonds denote the presence of Tcf1

binding peaks. Triangles filled with blue and red denote statistically significant decrease and increase in CTCF binding strength in dKO $CD8^+$ T cells, respectively.

Figure S7 (related to Figure 5 and 7). Analyses of pStat5a in WT and Tcf1/Lef1-deficient $CD8^+$ T cells before and after IL-7/15 stimulation.

A. PCA of pStat5a CUT&RUN libraries. pY694-Stat5a CUT&RUN was performed on naïve WT GFP^+ $CD8^+$ T cells, before stimulation, or after 3- or 24-hr stimulation with IL-7 and IL-15, and on dKO GFP^+ $CD8^+$ T cells after 24-hr stimulation, each in two replicates.

B. Venn diagram showing pStat5 binding peaks in WT $CD8^+$ T cells at 0-, 3- and 24-hr after IL-7/15 stimulation.

C. GO terms for genes linked to pStat5a peaks detected in 24-hr stimulated WT $CD8^+$ T cells using GREAT, with dot size denoting term enrichment and dot color denoting statistical significance.

D. Top motifs of pStat5a peaks detected in 24-hr stimulated WT $CD8^+$ T cells as determined with HOMER.

E. Visualization of WT-specific pStat5a binding sites, as marked with open bars with green edges, at select gene loci. Shown are Tcf1 ChIP-Seq tracks in naïve WT $CD8^+$ T cells (top), CTCF CUT&RUN in WT and dKO $CD8^+$ T cells before or after 72-hr IL-7/15 stimulation (middle 4), and pStat5a CUT&RUN tracked in WT and dKO $CD8^+$ T cells after 24-hr IL-7/15 stimulation (bottom 2). Whole or partial gene structure, transcription orientation and genomic scales are displayed on top of each panel.

STAR METHODS

RESOURCE AVAILABILITY

Lead contact. Further information and requests for resources and reagents should be directed to and will be fulfilled by the lead contact, Hai-Hui Xue (haihui.xue@hmh-cdi.org).

Materials availability. This study did not generate new unique reagents.

Data and code availability. The Hi-C, DNase-Seq, RNA-Seq, CTCF CUT&RUN, and Stat5 CUT&RUN data in IL-7/15-stimulated WT and dKO $CD8^+$ T cells, along with CTCF CUT&RUN in naïve WT and dKO $CD8^+$ T cells are under GSE179775. The token for the reviewers is snqtkeqwjlmpxub. The Hi-C, DNase-Seq, and RNA-Seq data in naïve WT and dKO $CD8^+$ T cells, Tcf1 ChIP-Seq data in naïve WT $CD8^+$ T cells are deposited at the Gene Expression Omnibus under accession number GSE164713, and are publicly available.

The HiCHub is publicly available at https://github.com/lux563624348/HiC_Hubs, version 0.2.0, DOI:10.5281/zenodo.5095330.

EXPERIMENTAL MODEL AND SUBJECT DETAILS

Mice. C57BL/6J (B6), B6.SJL, *Rag1*$^{-/-}$, hCD2-Cre, and Rosa26^{GFP} mice were from the Jackson Laboratory. *Tcf7*$^{FL/FL}$and *Lef1*$^{FL/FL}$ mice were previously described (Steinke et al.,

2014; Yu et al., 2012) and *Ctcf*$^{FL/FL}$ mice were provided by Drs. Niels Galjart (Erasmus University Medical Center, the Netherlands) and Ari Melnick (Weill Cornell Medicine) (Heath et al., 2008). All compound mouse strains used in this work were from in-house breeding at the animal care facilities of University of Iowa and Center for Discovery and Innovation, Hackensack University Medical Center. All mice, if not specifically mentioned in this manuscript, were 6–12 weeks of age, and both genders were used without randomization or blinding. All mouse experiments were performed under protocols approved by the Institutional Animal Use and Care Committees of the University of Iowa and Center for Discovery and Innovation, Hackensack University Medical Center.

METHOD DETAILS

Flow cytometry. Single-cell suspensions were prepared from the spleen, lymph nodes (LNs), and surface or intracellularly stained as described (Shan et al., 2017). The fluorochrome-conjugated antibodies were as follows: anti-CD4 (RM4-5), anti-CD8 (53-6.7), anti-TCRβ (H57-597), anti-CD45.1 (A20), anti-CD45.2 (104), anti-CD62L (MEL-14), anti-IL-2Rβ (TM-β1), anti-IL-7Rα (A7R34), anti-Eomes (Dan11mag) and anti-CD44 (IM7) were from Thermo Fisher Scientific; anti-γ_c (TUGm2) from BioLegend; anti-Tcf1 (C63D9) and anti-Lef1 (C12A5) from Cell Signaling Technology. For detection of Tcf1 and lef1, surface-stained cells were fixed and permeabilized with the Foxp3/Transcription Factor Staining Buffer Set (eBiosciences), followed by incubation with corresponding fluorochrome-conjugated antibodies. For detection of cell survival

status, the PE Annexin V Apoptosis Detection Kit (BD Biosciences) was used following the manufacturer's instruction. Data were collected on FACSCelesta or FACSVerse (BD Biosciences) and were analyzed with FlowJo software V10 (TreeStar).

Cell labeling, ex vivo culture, and adoptive transfer. For *in vivo* analyses, WT, Tcf1/Lef1-double deficient, or CTCF-deficient naïve $CD8^+$ T cells were enriched from spleen and lymph nodes by negative selection via depleting cells expressing CD4, B220, TER119, NK1.1, Gr1, CD11b, CD11c and CD44 using EasySep™ Biotin Positive Selection Kit II (StemCell Technology). The enriched cells were labeled with 10 μM Cell Trace Violet (CTV, Invitrogen/Life Sciences), 1×10^6 of CTV-labeled $CD45.2^+CD8^+$ cells were adoptively transferred into either lymphopenic hosts (i.e., sublethally irradiated $CD45.1^+$ B6.SJL or *Rag1*$^{-/-}$ mice) *via* tail vein injection. After 72 hrs, CTV dilution was detected on $CD45.2^+GFP^+CD8^+$ cells. In another experiment, the enriched naïve $CD45.2^+GFP^+CD8^+$ T cells were mixed at 1:1 ratio with $CD45.1^+$ WT $CD8^+$ competitor cells followed by adoptive transfer into $CD45.2^+$ B6.SJL replete hosts, and persistence of both donor cell types were tracked for 3 weeks.

For *ex vivo* analysis, the enriched $CD8^+$ cells were cultured in RPMI 1640 medium supplemented with 10% FBS, 2 mM L-glutamine, 100 U/ml penicillin–streptomycin, 1 mM HEPES, 1 mM sodium pyruvate, 50 μM β-mercaptoethanol, and stimulated with IL-7 and IL-15 (both at 50 ng/ml) for 0, 3, 24 or 72 hrs. The stimulated cells were sorted for viable cells with naïve phenotype ($CD44^{med\text{-}lo}CD62L^+$) and used in multiomics analyses. For tracking cell division *in vitro*, the enriched cells were CTV-labeled and stimulated with IL-7/15 or plate-bound anti-CD3 (10 μg/ml) + soluble anti-CD28 (1 μg/ml) + IL-2 (100 units/ml) for 72-96 hrs, and CTV dilution was tracked.

Immunoblotting and Immunoprecipitation. To detect intracellular signals activated by homeostatic cytokines, sorted naïve CD8 T cells were incubated with IL-7 and IL-15 (each at 50 ng/ml) for 0, 5, 15, 30, 60 and 180 minutes. The stimulation was stopped by addition of lysis buffer, and cell lysates were extracted and immunoblotted with the following antibodies: anti-pY694-STAT5a (clone: C11C5, Cell Signaling Technology), pS473-Akt (clone: 193H12, Cell Signaling Technology), total Stat5a (clone ST5a-2H2, ThermoFisher Scientific), and total Akt (C67E7, Cell Signaling Technology).

The cDNAs coding WT Stat5a or a constitutive active mutant Stat5a-1*6 were obtained from Dr. Warren Leonard (NHLBI, NIH) and cloned into Mig-R1 retroviral vector. Mig-R1 expressing N-terminal FLAG-tagged Tcf1 was previously described (Xing et al., 2016). To detect protein-protein interactions, the expression plasmids were transfected into 293T cells using Lipofectamine 2000 (Life Technologies). After 24 hrs, cell lysates were extracted, incubated with anti-CTCF serum (Millipore) overnight at 4^{o}C, followed by 2-hr incubation with Dynabeads Protein G (Life Technologies). the immunoprecipitated samples were immunoblotted with anti-Stat5 or anti-FLAG. In another experiment, the cell lysates were incubated with anti-FLAG M2 Magnetic Beads (Millipore) overnight, followed by immunoblotting with anti-CTCF or anti-Stat5a.

RNA-Seq and data analysis

Data generation. For cytokine-stimulated groups, $CD8^+$ T cells were first enriched by negative selection, cultured in the presence of IL-7 and IL-15 (each at 50 ng/ml) for 72 hrs, and then GFP^+CD8^+ T cells in $CD44^{med\text{-}lo}CD62L^+$ naïve phenotype were sorted. This protocol was adopted to avoid diminished viability and/or reduced responsiveness to

cytokines after cell sorting. Total RNA was extracted from the sorted cells (three biological replicates for each group), cDNA synthesis and amplification were performed using SMARTer Ultra Low Input RNA Kit (Clontech) following manufacturer's instruction. The resulting libraries were sequenced on Illumina's HiSeq2000 in single-end mode with the read length of 50 nucleotides. The RNA-Seq data for the stimulated $CD8^+$ T cells were deposited at the GEO (GSE179725) under the SuperSeries of GSE179775. The RNA-Seq data for the naïve $CD8^+$ T cells were previously reported (Shan et al., in press) and deposited at the GEO (GSE164712) under the SuperSeries of GSE164713.

Reproducibility analysis and dynamic transcriptome clustering. The sequencing quality of RNA-Seq libraries were assessed by FastQC (v0.11.4), and adaptors were removed through Cutadapt (Arce et al., 2006). The reads were mapped to mouse genome mm9 using Tophat (v2.1.0) (Kim et al., 2013). The expression level of a gene was expressed as a gene-level Fragments Per Kilobase of transcripts per Million mapped reads (FPKM) value. Mapped reads were then processed by Cuffdiff (v2.2.1) (Trapnell et al., 2012) to estimate expression levels of all genes and identify differentially expressed genes (DEGs) between a pair of conditions. The reproducibility of RNA-Seq data was evaluated by applying the Principal Component Analysis (PCA) for all genes. Pairwise DEGs in $CD8^+$ T cells were identified by requiring $\geq$ 2-fold expression changes and FDR < 0.05, as well as FPKM $\geq$ 1 in the higher expression samples. DEGs from 4 key comparisons (defined in **Fig. S3B**) were collected for analysis of dynamic transcriptomic changes. By applying K-means clustering to the row-wise z-score-transformed expression values of these genes, we obtained 7 clusters of genes with distinct dynamic patterns of expression (**Fig.**

2B). UCSC genes from the iGenome mouse mm9 assembly (http://support.illumina.com/sequencing/sequencing_ software/igenome.html) were used for gene annotation.

DNase-Seq and data analyses

Data generation. DNase-Seq was performed following detailed protocols described previously (Jin et al., 2015). In brief, WT or dKO $CD8^+$ T cells were stimulated with IL-7/15 for 72 hrs, and then sorted in 2 biological replicates each (3×10^5 cells/replicate). The cells were lysed in lysis buffer (10 mM Tris-HCl pH 7.5, 10 mM NaCl, and 3 mM $MgCl_2$) and digested with 2.4 units of DNase I at 37^{o}C for 5 min. The reaction was terminated by addition of stop buffer (10 mM Tris-HCl pH7.5, 10 mM NaCl, 10 mM EDTA, 2% SDS, 0.5 mg/ml Proteinase K, and 1 ng/ml of circular carrier DNA), and incubated at 65^{o}C for 1 hr. After purification with phenol-chloroform extraction and ethanol precipitation, the DNA was end-repaired using End-It DNA-Repair kit (Epicentre) at 37^{o}C for 20 min, and then treated with Klenow fragment (3'–>5' exo–, NEB) and dATP to yield a protruding A base at the 3' end. The DNA fragments were then ligated to the Illumina Paired End Adaptors, and amplified with PCR for library construction. PCR products between 160-300 bp were isolated on 2% E-gel for sequencing on Illumina HiSeq2000 in paired-end mode with the read length of 150 nucleotides. The DNase-Seq data for stimulated cells were deposited at the GEO (GSE179724) under the SuperSeries of GSE179775. The DNase-Seq data for naïve WT and dKO cells were previously reported (Shan et al., in press), and deposited the GEO (GSE164689) under the SuperSeries of GSE164713.

Data processing. The sequencing quality of DNase-Seq libraries was assessed by FastQC v0.11.4 (http://www.bioinformatics.babraham.ac.uk/projects/fastqc/). Bowtie2 v2.2.5 (Langmead and Salzberg, 2012) was used to align the sequencing reads to the mm9 mouse genome, and only uniquely mapped reads (MAPQ>10) were retained. Samtools 1.7 (Li et al., 2009) was used to transfer sam files to bam files and sort bam files. Picard MarkDuplicates 2.21.6-SNAPSHOT (https://github.com/broadinstitute/picard) was used to remove duplicate reads in bam files. MACS v2.1.1 (Zhang et al., 2008) was used for DNase I-hypersensitive site (DHS) peak calling with stringent criteria of ≥ 4 summit fold change, p-value < 1e–5 and FDR < 0.05. For DHS peaks in a given condition, the mapped reads from replicates were pooled for peak calling. For consistency, the DHS peaks are referred to as chromatin accessible (ChrAcc) sites in this work.

Reproducibility analysis. Peaks called by MACS2 in 9 libraries (*i.e.*, 3 naïve WT, 2 naïve dKO, 2 stimulated WT and 2 stimulated dKO libraries) were merged into 44,682 union peaks. Raw reads were counted in each library on the union peaks resulting in a 44,682 × 9 matrix with rows representing peaks and columns represents libraries. The raw-count matrix is then subject to row-wise normalization by peak length per kilobase and then column-wise normalization by the column sum per million. The normalized matrix is subject to PCA analysis with the z-score option.

***Identification of differential ChrAcc sites*.** The 44,682 × 9 raw count matrix was used as input for edgeR (v.3.28.1) (Robinson et al., 2010) (quasi-likelihood test, robust, fold-change >= 2 and FDR < 0.05) to identify differential ChrAcc sites between a pair of comparisons. To analyze ChrAcc dynamics, we focused on 5,202 differential ChrAcc sites from 4 key comparisons (**Fig. S3B**), and the corresponding 5,202 rows were

extracted from the normalized 44,682 × 9 matrix and subjected to row-wise z-score transformation. K-means clustering was then applied to separate these differential peaks into 6 clusters with distinct ChrAcc dynamics (**Fig. S4B**).

Identification of regulatory factor motifs from ChrAcc data. ChromVar (R package version 1.8.0) (Schep et al., 2017) was applied to the 44,682 × 9 matrix of merged ChrAcc sites with the default parameters and the motif database "mouse_pwms_v1". Variability of ChrAcc signal intensity across the 4 conditions for each motif was calculated by chromVar to identify regulatory factors that correlate with ChrAcc changes .

Correlation matrix for association of DEG and dynamic ChrAcc clusters. An observed count matrix was first calculated, with the matrix elements O_{ij} representing the observed number of genes in the j_{th} DEG cluster that was associated with the i_{th} cluster of the dynamic ChrAcc cluster, where a ChrAcc site localized in a gene body and its 50 kb flanking regions was considered to be associated with the gene. The element of the enrichment score matrix was then defined as the observed count O_{ij} divided by the expected count E_{ij}, which was calculated as $P_i Q_j \sum_{ij} Q_{ij}$, where $P_i = \sum_j O_{ij} / \sum_{ij} O_{ij}$ and $Q_j = \sum_i O_{ij} / \sum_{ij} O_{ij}$.

Tcf1 ChIP-Seq and data analysis. Tcf1 ChIP-Seq was performed on naïve $CD8^+$ T cells, and high confidence Tcf1 binding peaks were identified as previously described (Shan et al., in press).

CTCF CUT&RUN and data analyses

Data generation. Cleavage Under Targets and Release Using Nuclease (CUT&RUN) (Skene and Henikoff, 2017) was used to globally map CTCF binding sites in $CD8^+$ T cells in naïve state or after IL-7/IL-15 stimulation for 72 hrs. In brief, FACS-sorted live cells (1×10^5 cells/reaction) were bound to Concanavalin A coated magnetic beads (Bangs Laboratories), and permeabilized with 0.05% (w/v) digitonin, and then incubated with anti-CTCF antiserum (Active Motif, 1 µl/reaction) overnight. After removal of unbounded antibodies with proper washing, the nuclei were incubated with protein A/G-MNase fusion protein (plasmid obtained from Addgene) for one hour at 4°C. $CaCl_2$ was then added to activate MNase activity and incubated on ice for 30 min. The reaction was quenched with stopping buffer, and the DNA fragments were purified with MinElute Reaction Cleanup Kit (Qiagen), and then amplified by PCR for 10-14 cycles with barcoded Nextera primers (Illumina). DNA fragments in the range of 150-1,000 bp were recovered from 2% E-Gel EX Agarose Gels (Invitrogen/ThermoFisher Scientific). The libraries were quantified using a KAPA Library Quantification kit and sequenced on Illumina HiSeq X Five/Ten sequencing systems in paired end 150 bp reads at the Admera Health. The CTCF CUT&RUN data were deposited at the GEO (GSE179723) under the SuperSeries of GSE179775.

Data processing. The sequencing quality of the libraries was assessed by FastQC v0.11.9 (http://www.bioinformatics.babraham.ac.uk/projects/fastqc/). Trim Galore 0.6.4_dev (https://www.bioinformatics.babraham.ac.uk/projects/trim_galore/) was used to remove 25bp from the 3' end as well as adapter sequences. Bowtie2 v2.2.5 (Langmead and Salzberg, 2012) was used to align the sequencing reads to the mm9 mouse genome, and

only uniquely mapped reads (MAPQ>10) were retained. Samtools 1.7 (Li et al., 2009) was used to transfer the sam files to bam files and sort bam files. Picard MarkDuplicates 2.21.6-SNAPSHOT (https://github.com/broadinstitute/picard) was used to remove duplicate reads in the bam files. MACS v2.1.1 (Zhang et al., 2008) was used for CTCF peak calling, with the IgG CUT&RUN library in the naïve $CD8^+$ T cells used a negative control, where stringent criteria of ≥ 4 summit fold change, p-value < 1e–5 and FDR < 0.05 were used. CTCF binding events in a cell type/state were called by applying MACS2 to reads from biological replicates pooled together.

Reproducibility analysis. Significant peaks called by MACS2 from the 8 CTCF CUT&RUN libraries of four cell types/states were merged into 39,574 union peaks. Raw counts in each library were mapped onto those union peaks, resulting in a 39,574 $\times$ 8 matrix with rows representing the peaks and columns representing the libraries. The raw-count matrix was then subjected to normalization as follows: each row, representing a peak region, was normalized by length of each peak region per kilobase and each column, representing a library, was then normalized by the column sum per million. The normalized matrix was subjected to PCA analysis with the z-score option.

Identification of dynamic CTCF clusters. The 39,574 × 8 raw-count matrix was used as input for edgeR (v.3.28.1) (Robinson et al., 2010) (quasi-likelihood test, robust, fold-change >= 2 and FDR < 0.05) to identify differential CTCF binding sites between a pair of conditions. To analyze the dynamic changes in CTCF binding strength in four cell types/states, we collected the 6,876 differential CTCF peaks from the four key comparisons as defined in **Fig. S3B**, and the corresponding 6,876 rows were extracted from the normalized 39,574 × 8 matrix and subjected to row-wise z-score transformation.

K-means clustering was then applied to separate these differential CTCF peaks into 7 clusters with distinct CTCF binding dynamics (**Fig. 3C**).

Correlation matrix for association of DEG and dynamic CTCF clusters was generated following the same approach as described for dynamic ChrAcc clusters.

Defining local chromatin characteristics at CTCF and Tcf1 binding sites. The presence or absence of CTCF motif in CTCF or Tcf1 binding peaks was determined by motifmatchr (R package version 1.8.0) using the chromVar motif database "mouse_pwms_v1". The $Tcf1^{-}CTCF^{+}$motif+, $Tcf1^{-}CTCF^{+}$motif–, $Tcf1^{+}CTCF^{+}$motif+ sites were ordered by CTCF binding intensity, while $Tcf1^{+}CTCF^{+}$motif– sites were ordered by Tcf1 binding intensity. The CTCF, ChrAcc and H3K27ac profiles at distal sites were normalized by the number of reads on the peaks per million reads in each type of libraries. The H3K27ac ChIP-Seq data were previously reported (Shan et al., in press) and deposited at the GEO (GSE164711) under the SuperSeries of GSE164713. Mapped reads from replicates were pooled for identification of ChIP-enriched regions in a condition using SICER (v1.1) (Zang et al., 2009) with the setting of windows size = 200 bps, gap size = 400 bps and FDR < 0.01.

Phosphorylated Stat5a CUT&RUN and data analyses

Data generation. Naïve WT $CD8^{+}$ T cells were sort-purified and stimulated with IL-7/15 for 0, 3, or 24 hrs, and dKO $CD8^{+}$ T cells stimulated for 24 hrs. The cells were fixed with 1% formaldehyde at room temperature for 10 minutes, and then suspended in RIPA buffer. SDS was added to a final concentration of 0.2% to decondensate the chromatin, and incubated at room temperature for 10 minutes followed by washing with antibody

binding buffer (10 mM Tris-HCl pH7.5, 10 mM EDTA, 150 mM NaCl, and 0.1% Triton X-100). pY694-Stat5a antibody (0.5 µl/reaction) was incubated with protein A/G-MNase fusion protein on ice for 30 min and then added to the decondensated cell suspension (1×10^5 cells/reaction) followed by 1-hr incubation on ice. After removal of unbounded antibodies with proper washing, $CaCl_2$ was added to activate MNase activity and incubated at 37°C for 3 min. The reaction was stopped, and DNA fragments were used for library construction and sequenced as described for CTCF CUT&RUN. The pStat5a CUT&RUN data were deposited at the GEO (GSE179729) under the SuperSeries of GSE179775.

Data processing. The sequencing quality of the libraries was assessed by FastQC v0.11.9 (http://www.bioinformatics.babraham.ac.uk/projects/fastqc/). Trim Galore 0.6.4_dev (https://www.bioinformatics.babraham.ac.uk/projects/trim_galore/) was used to remove 25 bp from the 3' end as well as adapter sequences. Bowtie2 v2.2.5 (Langmead and Salzberg, 2012) was used to align the sequencing reads to the mm9 mouse genome, and only uniquely mapped reads (MAPQ>10) were retained. Samtools 1.7 (Li et al., 2009) was used to transfer the sam files to bam files and sort bam files. Picard MarkDuplicates 2.21.6-SNAPSHOT (https://github.com/broadinstitute/picard) was used to remove duplicate reads in the bam files. MACS v2.1.1 (Zhang et al., 2008) was used for pStat5 peak calling using genome as background. Stringent criteria of ≥ 4 summit fold change, p-value < 1e–5 and FDR < 0.05 were used for significance. pStat5 binding events in a given condition were called by applying MACS2 to reads from biological replicates pooled together.

Reproducibility analysis. Significant pStat5a peaks called by MACS2 from eight Stat5 CUT&RUN libraries (two replicates each for WT cells after 0, 3, and 24 hr stimulation and dKO cells after 24 hr stimulation) were merged into 28,326 union peaks. Raw counts in each library were mapped onto those union peaks, resulting in a 28,326 × 8 matrix with rows representing the peaks and columns representing the libraries. The raw-count matrix was then subjected to normalization as follows: each row, representing a peak region, was normalized by length of each peak region per kilobase, and each column, representing a library, was then normalized by the column sum per million. The normalized matrix was subjected to PCA analysis with the z-score.

Identification of differential pStat5a binding sites. pStat5a peaks from WT and dKO $CD8^+$ T cells stimulated with IL-7/15 for 24 hrs (two replicates each) were merged into 27,717 union peaks. Reads from the 4 libraries were mapped on to the union peaks, resulting into a 27,717 × 4 raw-count matrix. The matrix was then used as input for edgeR (v.3.28.1) (Robinson et al., 2010) (quasi-likelihood test, robust, fold-change >= 2 and p-value < 0.05) to identify differential pStat5a binding sites between 24 hr-stimulated WT and dKO $CD8^+$ T cells.

High-resolution chromosome-conformation-capture (Hi-C) and data analyses

Hi-C data generation. Hi-C was performed using the three enzyme Hi-C (3e Hi-C) approach as previously described (Ren et al., 2017). In brief, WT and dKO $CD8^+$ T cells that were stimulated with IL-7/15 for 72 hrs (each in two replicates, 4×10^6 cells/replicate) were sorted and cross-linked with 1% formaldehyde for 10 minutes at 25ºC. The crosslinked cells were lysed in 10 ml lysis buffer (10 mM Tris-HCl pH 8.0, 10 mM NaCl,

0.2% NP-40) supplemented with protease inhibitor cocktail (Millipore/Sigma) at 4ºC for 1 hr. The nuclei were collected and treated with 400 µl 1×CutSmart buffer (NEB) containing 0.1% SDS at 65ºC for 10 minutes, and Triton X-100 was added to a final concentration of 1% to quench SDS. The resulting chromatin was then digested with three restriction enzymes, CviQ I, CviA II, and Bfa I (NEB), at 20 units each at 37ºC for 20 minutes. The reaction was stopped by washing with 600 µl wash buffer (10 mM NaCl, 1 mM EDTA, 0.1% Triton X-100) two times. The DNA ends were blunted and labeled with biotin by Klenow enzyme in the presence of dCTP, dGTP, dTTP, biotin-14-dATP, followed by ligation using T4 DNA ligase. After reverse crosslinking, DNA was fragmented by sonication with a Covaris S2 ultrasonicator. The DNA fragments were then end-repaired, and the biotinylated DNA fragments were captured using Dynabeads MyOne Streptavidin C1 beads (Invitrogen, Thermo Fisher Scientific). The DNA on beads was ligated to the Illumina Paired End Adaptors, and amplified with PCR for library construction. DNA fragments of 300-700 bp were purified from 2% E-gel and sequenced on HiSeq4000 in paired read mode with the read length of 150 nucleotides. The Hi-C data for WT and dKO $CD8^+$ T cells in naïve state were previously reported (Shan et al., in press) and deposited at the GEO (GSE164710) under the SuperSeries of GSE164713. The Hi-C data for stimulated WT and dKO $CD8^+$ T cells were deposited at the GEO (GSE179773) under the SuperSeries of GSE179775.

Hi-C library mapping. Iterative_mapping from 25 bps to 105 bps with a step size of 5 bps using hiclib (https://github.com/mirnylab/hiclib-legacy) was applied to the Hi-C sequencing libraries for alignment onto reference genome mm9. Picard (http://broadinstitute.github.io/picard/) was then applied for redundancy removal. The

resulting libraries were subjected to further processing using Mirnylib with default parameters except filterDuplicates (mode='ram') (https://github.com/mirnylab/hiclib-legacy) into hdf5 file. The hdf5 files were converted into text files and then .hic files using the Juicer (Durand et al., 2016) pre function. The .hic file is a highly compressed binary file that provides rapid random access to the binned matrices at 9 resolutions: 2.5 m, 1m, 500 k, 250 k, 100 k, 50 k, 25 k, 10 k, and 5 k base pairs.

Reproducibility of Hi-C replicates. The binned contact matrices were converted into a text file using the straw function in Juicer v1.21.01 (Durand et al., 2016) with parameters (observed; delimited: base-pair; resolution:10kb; normalization: distance normalization, see below). For each anchor and each replicate, the respective row sum of the contact matrix elements (excluding the diagonal element) was calculated. Scatterplots of the resulting data were used to calculate the Pearson correlation of the replicates.

Identification of topological associated domains (TADs). TADs were identified by the Arrowhead algorithm from Juicer v1.21.01 (Durand et al., 2016) using the medium resolution maps (*i.e.*, m: 2000; resolution: 10kb; normalization: KR). A total of 1,724 TADs were identified in WT naive $CD8^+$ T cells using the pooled Hi-C data, which were used to determine distribution of $Tcf1^+CTCF^+$ cobound sites and CTCF solo sites.

Distance normalization of the contact matrix. The raw-count contact matrix was subjected to distance normalization (Fang et al., 2020) as follows. For a matrix element M_{ij} with $|i-j| = d$, we counted the number of elements N_d with the same distance d in the same chromosome $N_d = \sum_{i,|i-j|=d} 1$. The average interaction of distance d on the same chromosome was $S_d = \sum_{i,|i-j|=d} \mathrm{M_{ij}} / \mathrm{N_d}$. The normalized matrix element was

defined as $\widehat{M}_{ij} = M_{ij}/S_d$. The distance normalized contact matrices were used for the downstream analysis and visualization unless specified otherwise.

Calculation of insulation index. We calculated the insulation score using the matrix2insulation script (Crane et al., 2015). To make the result more intuitive, we defined an insulation index as (- insulation score +1), where higher insulation index corresponded to higher insulation effects.

Calculation of interaction score of an anchor. For an anchor, the sum of its distance normalized interaction with other bins on the same chromosome was defined as the interaction score.

HiCHub, a network approach for comparing chromatin interactions between two cell types/states. We devised a network approach to systematically compare chromatin interaction differences between two experimental conditions (cell types/states). A comparison between WT and dKO naïve $CD8^+$ T cells is used here to illustrate the analytical procedures. 1) Normalization. To enable fair comparison, we normalized the two raw contact matrices (resolution:10 kb) based on the assumption that the majority of interactions at any distance are unchanged. Specifically, for each contact matrix element, the geometric mean of WT and dKO interaction values was calculated, the matrix elements were then stratified according to the geometric mean values. For each stratified region, the sum of the elements within that region was taken for WT and dKO cells, respectively. The ratio of the sums was used as the normalization factor and applied to the dKO contact matrix. After the normalization, the distribution of Log_2(dKO/WT) for every stratified region was expected be centered around zero. 2) Network clustering. The normalized matrices were then used to identify cell type/state-specific chromatin

interaction hubs. For example, to identify naïve WT-specific hubs in comparison with naïve dKO $CD8^+$ T cells, chromatin interactions that showed decrease in dKO over WT naïve $CD8^+$ T cells were selected to construct a network using the igraph platform. Clusters on the network were identified using the community_multilevel algorithm (Blondel et al., 2008) (weights = WT- dKO interaction frequency, return_levels = 1). 3) Projection to genome. The network clusters were then projected onto the genome to identify genomic regions (*i.e.*, candidate hubs) as follows. The network nodes correspond to the genomic bins. For each network cluster, each bin was scored by the pagerank value of the corresponding network node. Bins with pagerank value higher than the chromosomal median of pagerank values were designated as legitimate and subject to stitching along the genome allowing gaps of up to 1 bin. The resulting stitched regions became candidate hubs. 4) Significance evaluation. For each pair of the projected candidate hubs (including self), interactions connecting the two regions were collected and one-sided Wilcoxon signed rank test was used to calculate the significance of changes of these interactions. Only candidates with p-value < 1.0e–8 were considered as naïve WT-specific hubs. The hubs specific in another cell type/state were identified following the same procedure by focusing on chromatin interactions that showed increase in that cell type/state. The promoters of DEGs from the two cell types/states were then stratified against cell type/state-specific hubs to identify genes whose expression was evidently modulated by changes in chromatin interaction network.

QUANTIFICATION AND STATISTICAL ANALYSIS

For comparison between two experimental groups, Student's *t*-test was used. For multiple group comparisons, one-way ANOVA was used to first determine whether any of the differences between the means are statistically significant. As post hoc correction, Tukey's test was used to determine statistically significance between two groups of interest. Statistical analyses in multiomics data processing were defined above. The statistical significance for the multiomics analyses was determined using the processing algorithms. Specifically, Cuffdiff was used for RNA-seq, MACS2 for DNase-Seq, CTCF and pStat5a CUT&RUN , and SICER for H3K27ac ChIP-Seq. The statistical significance of differential hubs was determined using HicHub, and that associated with gene pathway and ontology analysis was determined by DAVID and GREAT, and that for motif analysis was determined by HOMER. For comparisons between two sets of data points in boxplots, one-sided Mann-Whitney U test was used. For enrichment analysis, one-sided binomial test was used.

KEY RESOURCES TABLE

REAGENT or RESOURCE	SOURCE	IDENTIFIER
Antibodies		
Antibodies for flow cytometry		
anti-CD4 antibody	Thermo Fisher Scientific	clone: RM4-5; RPID: AB_2536064
anti-CD8 antibody	Thermo Fisher Scientific	clone: 53-6.7; RPID: AB_2534400
anti-CD45.1 antibody	Thermo Fisher Scientific	clone: A20; RPID: AB_465675
anti-CD45.2 antibody	Thermo Fisher Scientific	clone: 104; RPID: AB_953590
anti-CD62L antibody	Thermo Fisher Scientific	clone: MEL-14; RPID: AB_2534236
anti-IL-2Rβ antibody	Thermo Fisher Scientific	clone: TM-β1; RPID: AB_465836
anti-IL-7Rα antibody	Thermo Fisher Scientific	clone: A7R34; RPID: AB_469435
anti-Eomes antibody	Thermo Fisher Scientific	clone: Dan11mag; RPID: AB_2573454
anti-CD44 antibody	Thermo Fisher Scientific	clone: IM7; RPID: AB_925746
anti-TCRβ antibody	BioLegend	clone: H57-597; RPID: AB_1027649
Anti-γc antibody	BioLegend	clone: TUGm2; RPID: AB_2280163
anti-TCF1 antibody	Cell Signaling Technology	clone: C63D9; RPID: AB_2798483
anti-LEF1 antibody	Cell Signaling Technology	clone: C12A5; RPID: AB_2798481
Antibodies for immunoprecipitation or western blot		
anti-pY694-STAT5a antibody	Cell Signaling Technology	clone: C11C5; RPID: AB_823649
anti-Stat5a antibody	Thermo Fisher Scientific	clone: ST5a-2H2; RPID: AB_2533013
anti-pS473-Akt antibody	Cell Signaling Technology	clone: 193H12; RPID: AB_915783
anti-AKT antibody	Cell Signaling Technology	clone: C67E7; RPID: AB_331168
anti-Flag M2 antibody	Sigma-Aldrich	clone: M2; RPID: AB_439685
anti-HA antibody	Cell Signaling Technology	clone: C29F4; RPID: AB_10693385
Antibodies for ex vivo stimulation		
anti-CD28 antibody	BD Biosciences	clone: 37.51; RPID: AB_396676
anti-CD3 antibody	In house	clone: 145-2C11
Antibodies for CUT&RUN		
anti-CTCF antibody	Millipore	Cat#: 07-729; RPID: AB_441965
anti-pY694-STAT5a antibody	Cell Signaling Technology	clone: C11C5; RPID: AB_823649
Chemicals, peptides, and recombinant proteins		
Recombinant Murine IL-7	Peprotech	Cat#: 217-17
Recombinant Murine IL-15	Peprotech	Cat#: 210-15
Recombinant Human IL-2	Peprotech	Cat#: 200-02
CellTrace™ Violet Cell Proliferation Kit	Thermo Fisher Scientific	Cat#: C34557
PE Annexin V Apoptosis Detection Kit	BD Biosciences	Cat#: 559763
Anti-FLAG® M2 Magnetic Beads	Sigma-Aldrich	Cat#: M8823
Deposited data		
RNA-Seq Data	GEO	GSE179725
CTCF CUT&RUN Data	GEO	GSE179723
pStat5a CUT&RUN Data	GEO	GSE179729
DNase-Seq Data	GEO	GSE179724
HiC Data	GEO	GSE179773
Experimental models: Cell lines		
HEK 293T cell	ATCC	Cat#: CRL-3216

Experimental models: Organisms/strains		
C57BL/6J mice	Jackson Laboratories	JAX stock #000664
Rag1$^{-/-}$ mice	Jackson Laboratories	JAX stock #34159
B6.SJL mice	Jackson Laboratories	JAX stock #000686
Rosa26GFP mice	Jackson Laboratories	JAX stock #032087
hCD2-Cre mice	Jackson Laboratories	JAX stock #027406
Tcf7 $^{FL/FL}$ mice	Made in house	PMC4064003
Lef1 $^{FL/FL}$ mice	Jackson Laboratories	JAX stock #030908
Ctcf $^{FL/FL}$ mice	Drs. Niels Galjart	PMC2580790
cDNA and Plasmid		
Stat5a-1*6 cDNA	Dr. Warren J. Leonard	
Stat5a cDNA	Dr. Warren J. Leonard	
FLAG-tagged Tcf1 cDNA	Made in house	PMC4873337
CTCF cDNA	Addgene	Cat#: 40801
MIGR1 plasmid	Addgene	Cat#: 27490
pAG/MNase plasmid	Addgene	Cat#: 123461
Software and algorithms		
FastQC v0.11.4	http://www.bioinformatics.babraham.ac.uk/projects/fastqc	
Cutadapt v1.18	https://cutadapt.readthedocs.io/en/stable/	
Trim_galore v1.18	https://www.bioinformatics.babraham.ac.uk/projects/trim_galore/	
Tophat v2.1.0	https://ccb.jhu.edu/software/tophat/index.shtml	
Cuffdiff v2.2.1	http://cole-trapnell-lab.github.io/cufflinks/cuffdiff/	
Bowtie2 v2.2.5	http://bowtie-bio.sourceforge.net/bowtie2/index.shtml	
Samtools v1.7	http://www.htslib.org/	
Picard v2.21.6	https://github.com/broadinstitute/picard	
MACS v2.1.1	https://github.com/macs3-project/MACS	
edgeR v.3.28.1	https://bioconductor.org/packages/release/bioc/html/edgeR.html	
Juicer v1.21.01	https://github.com/aidenlab/juicer	
ChromVar v1.8.0	https://github.com/GreenleafLab/chromVAR	
Motifmatchr v1.8.0	https://bioconductor.org/packages/release/bioc/html/motifmatchr.html	
Homer v4.11.1	http://homer.ucsd.edu/homer/motif/	
Hiclib	https://github.com/mirnylab/hiclib-legacy	
Matrix2insulation.pl	https://github.com/dekkerlab/crane-nature-2015	

.

References

Arce, L., Yokoyama, N.N., and Waterman, M.L. (2006). Diversity of LEF/TCF action in development and disease. Oncogene *25*, 7492-7504.

Arzate-Mejia, R.G., Recillas-Targa, F., and Corces, V.G. (2018). Developing in 3D: the role of CTCF in cell differentiation. Development *145*.

Banani, S.F., Lee, H.O., Hyman, A.A., and Rosen, M.K. (2017). Biomolecular condensates: organizers of cellular biochemistry. Nat Rev Mol Cell Biol *18*, 285-298.

Berard, M., Brandt, K., Bulfone-Paus, S., and Tough, D.F. (2003). IL-15 promotes the survival of naive and memory phenotype CD8+ T cells. J Immunol *170*, 5018-5026.

Blondel, V., Guillaume, J., Lambiotte, R., and Lefebvre, E. (2008). Fast unfolding of communities in large networks. Journal of Statistical Mechanics: Theory and Experiment *2008*, 10008.

Chisolm, D.A., Savic, D., Moore, A.J., Ballesteros-Tato, A., Leon, B., Crossman, D.K., Murre, C., Myers, R.M., and Weinmann, A.S. (2017). CCCTC-Binding Factor Translates Interleukin 2- and alpha-Ketoglutarate-Sensitive Metabolic Changes in T Cells into Context-Dependent Gene Programs. Immunity *47*, 251-267 e257.

Crane, E., Bian, Q., McCord, R.P., Lajoie, B.R., Wheeler, B.S., Ralston, E.J., Uzawa, S., Dekker, J., and Meyer, B.J. (2015). Condensin-driven remodelling of X chromosome topology during dosage compensation. Nature *523*, 240-244.

Dall'Agnese, A., Caputo, L., Nicoletti, C., di Iulio, J., Schmitt, A., Gatto, S., Diao, Y., Ye, Z., Forcato, M., Perera, R., *et al.* (2019). Transcription Factor-Directed Re-wiring of Chromatin Architecture for Somatic Cell Nuclear Reprogramming toward trans-Differentiation. Mol Cell *76*, 453-472 e458.

Di Fiore, B., and Pines, J. (2007). Emi1 is needed to couple DNA replication with mitosis but does not regulate activation of the mitotic APC/C. J Cell Biol *177*, 425-437.

Durand, N.C., Shamim, M.S., Machol, I., Rao, S.S., Huntley, M.H., Lander, E.S., and Aiden, E.L. (2016). Juicer Provides a One-Click System for Analyzing Loop-Resolution Hi-C Experiments. Cell Syst *3*, 95-98.

Emmanuel, A.O., Arnovitz, S., Haghi, L., Mathur, P.S., Mondal, S., Quandt, J., Okoreeh, M.K., Maienschein-Cline, M., Khazaie, K., Dose, M., *et al.* (2018). TCF-1 and HEB cooperate to establish the epigenetic and transcription profiles of CD4(+)CD8(+) thymocytes. Nat Immunol *19*, 1366-1378.

Fang, C., Wang, Z., Han, C., Safgren, S.L., Helmin, K.A., Adelman, E.R., Serafin, V., Basso, G., Eagen, K.P., Gaspar-Maia, A., *et al.* (2020). Cancer-specific CTCF binding facilitates oncogenic transcriptional dysregulation. Genome Biol *21*, 247.

Giese, K., Kingsley, C., Kirshner, J.R., and Grosschedl, R. (1995). Assembly and function of a TCR alpha enhancer complex is dependent on LEF-1-induced DNA bending and multiple protein-protein interactions. Genes Dev *9*, 995-1008.

Gong, Y., Lazaris, C., Sakellaropoulos, T., Lozano, A., Kambadur, P., Ntziachristos, P., Aifantis, I., and Tsirigos, A. (2018). Stratification of TAD boundaries reveals preferential insulation of super-enhancers by strong boundaries. Nat Commun *9*, 542.

Grosschedl, R., Giese, K., and Pagel, J. (1994). HMG domain proteins: architectural elements in the assembly of nucleoprotein structures. Trends Genet *10*, 94-100.

He, B., Xing, S., Chen, C., Gao, P., Teng, L., Shan, Q., Gullicksrud, J.A., Martin, M.D., Yu, S., Harty, J.T., *et al.* (2016). CD8(+) T Cells Utilize Highly Dynamic Enhancer Repertoires and Regulatory Circuitry in Response to Infections. Immunity *45*, 1341-1354.

Heath, H., Ribeiro de Almeida, C., Sleutels, F., Dingjan, G., van de Nobelen, S., Jonkers, I., Ling, K.W., Gribnau, J., Renkawitz, R., Grosveld, F., *et al.* (2008). CTCF regulates cell cycle progression of alphabeta T cells in the thymus. EMBO J *27*, 2839-2850.

Heinz, S., Benner, C., Spann, N., Bertolino, E., Lin, Y.C., Laslo, P., Cheng, J.X., Murre, C., Singh, H., and Glass, C.K. (2010). Simple combinations of lineage-determining transcription factors prime cis-regulatory elements required for macrophage and B cell identities. Mol Cell *38*, 576-589.

Hnisz, D., Shrinivas, K., Young, R.A., Chakraborty, A.K., and Sharp, P.A. (2017). A Phase Separation Model for Transcriptional Control. Cell *169*, 13-23.

Hu, G., Cui, K., Fang, D., Hirose, S., Wang, X., Wangsa, D., Jin, W., Ried, T., Liu, P., Zhu, J., *et al.* (2018). Transformation of Accessible Chromatin and 3D Nucleome Underlies Lineage Commitment of Early T Cells. Immunity *48*, 227-242 e228.

Huang da, W., Sherman, B.T., and Lempicki, R.A. (2009). Systematic and integrative analysis of large gene lists using DAVID bioinformatics resources. Nat Protoc *4*, 44-57.

Huber, W., Carey, V.J., Gentleman, R., Anders, S., Carlson, M., Carvalho, B.S., Bravo, H.C., Davis, S., Gatto, L., Girke, T., *et al.* (2015). Orchestrating high-throughput genomic analysis with Bioconductor. Nat Methods *12*, 115-121.

Im, S.J., Hashimoto, M., Gerner, M.Y., Lee, J., Kissick, H.T., Burger, M.C., Shan, Q., Hale, J.S., Lee, J., Nasti, T.H., *et al.* (2016). Defining CD8+ T cells that provide the proliferative burst after PD-1 therapy. Nature *537*, 417-421.

Jeannet, G., Boudousquie, C., Gardiol, N., Kang, J., Huelsken, J., and Held, W. (2010). Essential role of the Wnt pathway effector Tcf-1 for the establishment of functional CD8 T cell memory. Proc Natl Acad Sci U S A *107*, 9777-9782.

Jin, W., Tang, Q., Wan, M., Cui, K., Zhang, Y., Ren, G., Ni, B., Sklar, J., Przytycka, T.M., Childs, R., *et al.* (2015). Genome-wide detection of DNase I hypersensitive sites in single cells and FFPE tissue samples. Nature *528*, 142-146.

Johnson, J.L., Georgakilas, G., Petrovic, J., Kurachi, M., Cai, S., Harly, C., Pear, W.S., Bhandoola, A., Wherry, E.J., and Vahedi, G. (2018). Lineage-Determining Transcription Factor TCF-1 Initiates the Epigenetic Identity of T Cells. Immunity *48*, 243-257 e210.

Kim, D., Pertea, G., Trapnell, C., Pimentel, H., Kelley, R., and Salzberg, S.L. (2013). TopHat2: accurate alignment of transcriptomes in the presence of insertions, deletions and gene fusions. Genome Biol *14*, R36.

Langmead, B., and Salzberg, S.L. (2012). Fast gapped-read alignment with Bowtie 2. Nat Methods *9*, 357-359.

Leonard, W.J., Lin, J.X., and O'Shea, J.J. (2019). The gammac Family of Cytokines: Basic Biology to Therapeutic Ramifications. Immunity *50*, 832-850.

Leong, Y.A., Chen, Y., Ong, H.S., Wu, D., Man, K., Deleage, C., Minnich, M., Meckiff, B.J., Wei, Y., Hou, Z., *et al.* (2016). CXCR5(+) follicular cytotoxic T cells control viral infection in B cell follicles. Nat Immunol *17*, 1187-1196.

Li, F., Zhao, X., Zhang, Y., Shao, P., Ma, X., Paradee, W.J., Liu, C., Wang, J., and Xue, H.H. (2021). TFH cells depend on Tcf1-intrinsic HDAC activity to suppress CTLA4 and guard B-cell help function. Proc Natl Acad Sci U S A *118*.

Li, H., Handsaker, B., Wysoker, A., Fennell, T., Ruan, J., Homer, N., Marth, G., Abecasis, G., Durbin, R., and Genome Project Data Processing, S. (2009). The Sequence Alignment/Map format and SAMtools. Bioinformatics *25*, 2078-2079.

Li, P., Mitra, S., Spolski, R., Oh, J., Liao, W., Tang, Z., Mo, F., Li, X., West, E.E., Gromer, D., *et al.* (2017). STAT5-mediated chromatin interactions in superenhancers activate IL-2 highly inducible genes: Functional dissection of the Il2ra gene locus. Proc Natl Acad Sci U S A *114*, 12111-12119.

Lin, J.X., and Leonard, W.J. (2019). Fine-Tuning Cytokine Signals. Annu Rev Immunol *37*, 295-324.

Lin, J.X., Li, P., Liu, D., Jin, H.T., He, J., Ata Ur Rasheed, M., Rochman, Y., Wang, L., Cui, K., Liu, C., *et al.* (2012). Critical Role of STAT5 transcription factor tetramerization for cytokine responses and normal immune function. Immunity *36*, 586-599.

Love, J.J., Li, X., Case, D.A., Giese, K., Grosschedl, R., and Wright, P.E. (1995). Structural basis for DNA bending by the architectural transcription factor LEF-1. Nature *376*, 791-795.

Madsen, J.G.S., Madsen, M.S., Rauch, A., Traynor, S., Van Hauwaert, E.L., Haakonsson, A.K., Javierre, B.M., Hyldahl, M., Fraser, P., and Mandrup, S. (2020). Highly interconnected enhancer communities control lineage-determining genes in human mesenchymal stem cells. Nat Genet *52*, 1227-1238.

McLane, L.M., Abdel-Hakeem, M.S., and Wherry, E.J. (2019). CD8 T Cell Exhaustion During Chronic Viral Infection and Cancer. Annu Rev Immunol *37*, 457-495.

McLean, C.Y., Bristor, D., Hiller, M., Clarke, S.L., Schaar, B.T., Lowe, C.B., Wenger, A.M., and Bejerano, G. (2010). GREAT improves functional interpretation of cis-regulatory regions. Nat Biotechnol *28*, 495-501.

Nishimura, H., Yajima, T., Muta, H., Podack, E.R., Tani, K., and Yoshikai, Y. (2005). A novel role of CD30/CD30 ligand signaling in the generation of long-lived memory CD8+ T cells. J Immunol *175*, 4627-4634.

Ohlsson, R., Renkawitz, R., and Lobanenkov, V. (2001). CTCF is a uniquely versatile transcription regulator linked to epigenetics and disease. Trends Genet *17*, 520-527.

Ong, C.T., and Corces, V.G. (2014). CTCF: an architectural protein bridging genome topology and function. Nat Rev Genet *15*, 234-246.

Onishi, M., Nosaka, T., Misawa, K., Mui, A.L., Gorman, D., McMahon, M., Miyajima, A., and Kitamura, T. (1998). Identification and characterization of a constitutively active STAT5 mutant that promotes cell proliferation. Mol Cell Biol *18*, 3871-3879.

Philip, M., Fairchild, L., Sun, L., Horste, E.L., Camara, S., Shakiba, M., Scott, A.C., Viale, A., Lauer, P., Merghoub, T., *et al.* (2017). Chromatin states define tumour-specific T cell dysfunction and reprogramming. Nature *545*, 452-456.

Piazza, R., Magistroni, V., Redaelli, S., Mauri, M., Massimino, L., Sessa, A., Peronaci, M., Lalowski, M., Soliymani, R., Mezzatesta, C., *et al.* (2018). SETBP1 induces transcription of a network of development genes by acting as an epigenetic hub. Nat Commun *9*, 2192.

Pongubala, J.M.R., and Murre, C. (2021). Spatial Organization of Chromatin: Transcriptional Control of Adaptive Immune Cell Development. Front Immunol *12*, 633825.

Qi, Q., Cheng, L., Tang, X., He, Y., Li, Y., Yee, T., Shrestha, D., Feng, R., Xu, P., Zhou, X., *et al.* (2021). Dynamic CTCF binding directly mediates interactions among cis-regulatory elements essential for hematopoiesis. Blood *137*, 1327-1339.

Ren, G., Jin, W., Cui, K., Rodrigez, J., Hu, G., Zhang, Z., Larson, D.R., and Zhao, K. (2017). CTCF-Mediated Enhancer-Promoter Interaction Is a Critical Regulator of Cell-to-Cell Variation of Gene Expression. Mol Cell *67*, 1049-1058 e1046.

Robinson, M.D., McCarthy, D.J., and Smyth, G.K. (2010). edgeR: a Bioconductor package for differential expression analysis of digital gene expression data. Bioinformatics *26*, 139-140.

Schep, A.N., Wu, B., Buenrostro, J.D., and Greenleaf, W.J. (2017). chromVAR: inferring transcription-factor-associated accessibility from single-cell epigenomic data. Nat Methods *14*, 975-978.

Schluns, K.S., Kieper, W.C., Jameson, S.C., and Lefrancois, L. (2000). Interleukin-7 mediates the homeostasis of naive and memory CD8 T cells in vivo. Nat Immunol *1*, 426-432.

Shan, Q., Hu, S., Chen, X., Danahy, D.B., Badovinac, V.P., Zang, C., and Xue, H.H. (2021). Ectopic Tcf1 expression instills a stem-like program in exhausted CD8(+) T cells to enhance viral and tumor immunity. Cell Mol Immunol *18*, 1262-1277.

Shan, Q., Li. X., Chen, X., Zeng, Z., Zhu, S, Gai, K., Peng, W., and Xue, H.H. (2021) Tcf1 and Lef1 orchestrate genomic architecture to supervise mature $CD8^+$ T cell identity. Nat Commun, in press.

Shan, Q., Zeng, Z., Xing, S., Li, F., Hartwig, S.M., Gullicksrud, J.A., Kurup, S.P., Van Braeckel-Budimir, N., Su, Y., Martin, M.D., *et al.* (2017). The transcription factor Runx3 guards cytotoxic CD8(+) effector T cells against deviation towards follicular helper T cell lineage. Nat Immunol *18*, 931-939.

Shlyueva, D., Stampfel, G., and Stark, A. (2014). Transcriptional enhancers: from properties to genome-wide predictions. Nat Rev Genet *15*, 272-286.

Skene, P.J., and Henikoff, S. (2017). An efficient targeted nuclease strategy for high-resolution mapping of DNA binding sites. Elife *6*.

Staal, F.J., Luis, T.C., and Tiemessen, M.M. (2008). WNT signalling in the immune system: WNT is spreading its wings. Nat Rev Immunol *8*, 581-593.

Steinke, F.C., Yu, S., Zhou, X., He, B., Yang, W., Zhou, B., Kawamoto, H., Zhu, J., Tan, K., and Xue, H.H. (2014). TCF-1 and LEF-1 act upstream of Th-POK to promote the CD4(+) T cell fate and interact with Runx3 to silence Cd4 in CD8(+) T cells. Nat Immunol *15*, 646-656.

Surh, C.D., and Sprent, J. (2008). Homeostasis of naive and memory T cells. Immunity *29*, 848-862.

Takada, K., and Jameson, S.C. (2009). Naive T cell homeostasis: from awareness of space to a sense of place. Nat Rev Immunol *9*, 823-832.

Tan, J.T., Dudl, E., LeRoy, E., Murray, R., Sprent, J., Weinberg, K.I., and Surh, C.D. (2001). IL-7 is critical for homeostatic proliferation and survival of naive T cells. Proc Natl Acad Sci U S A *98*, 8732-8737.

Trapnell, C., Hendrickson, D.G., Sauvageau, M., Goff, L., Rinn, J.L., and Pachter, L. (2013). Differential analysis of gene regulation at transcript resolution with RNA-seq. Nat Biotechnol *31*, 46-53.

Trapnell, C., Roberts, A., Goff, L., Pertea, G., Kim, D., Kelley, D.R., Pimentel, H., Salzberg, S.L., Rinn, J.L., and Pachter, L. (2012). Differential gene and transcript expression analysis of RNA-seq experiments with TopHat and Cufflinks. Nat Protoc *7*, 562-578.

Utzschneider, D.T., Charmoy, M., Chennupati, V., Pousse, L., Ferreira, D.P., Calderon-Copete, S., Danilo, M., Alfei, F., Hofmann, M., Wieland, D., *et al.* (2016). T Cell Factor 1-Expressing Memory-like CD8(+) T Cells Sustain the Immune Response to Chronic Viral Infections. Immunity *45*, 415-427.

Velardi, E., Tsai, J.J., and van den Brink, M.R.M. (2021). T cell regeneration after immunological injury. Nat Rev Immunol *21*, 277-291.

Williams, M.A., and Bevan, M.J. (2007). Effector and memory CTL differentiation. Annu Rev Immunol *25*, 171-192.

Wolf, T., Jin, W., Zoppi, G., Vogel, I.A., Akhmedov, M., Bleck, C.K.E., Beltraminelli, T., Rieckmann, J.C., Ramirez, N.J., Benevento, M., *et al.* (2020). Dynamics in protein translation sustaining T cell preparedness. Nat Immunol *21*, 927-937.

Xing, S., Li, F., Zeng, Z., Zhao, Y., Yu, S., Shan, Q., Li, Y., Phillips, F.C., Maina, P.K., Qi, H.H., *et al.* (2016). Tcf1 and Lef1 transcription factors establish CD8(+) T cell identity through intrinsic HDAC activity. Nat Immunol *17*, 695-703.

Xue, H.H., and Zhao, D.M. (2012). Regulation of mature T cell responses by the Wnt signaling pathway. Ann N Y Acad Sci *1247*, 16-33.

Yao, Z., Cui, Y., Watford, W.T., Bream, J.H., Yamaoka, K., Hissong, B.D., Li, D., Durum, S.K., Jiang, Q., Bhandoola, A., *et al.* (2006). Stat5a/b are essential for normal lymphoid development and differentiation. Proc Natl Acad Sci U S A *103*, 1000-1005.
Yoshida, H., Lareau, C.A., Ramirez, R.N., Rose, S.A., Maier, B., Wroblewska, A., Desland, F., Chudnovskiy, A., Mortha, A., Dominguez, C., *et al.* (2019). The cis-Regulatory Atlas of the Mouse Immune System. Cell *176*, 897-912 e820.

Yu, S., Zhou, X., Steinke, F.C., Liu, C., Chen, S.C., Zagorodna, O., Jing, X., Yokota, Y., Meyerholz, D.K., Mullighan, C.G., *et al.* (2012). The TCF-1 and LEF-1 transcription factors have cooperative and opposing roles in T cell development and malignancy. Immunity *37*, 813-826.

Zamudio, A.V., Dall'Agnese, A., Henninger, J.E., Manteiga, J.C., Afeyan, L.K., Hannett, N.M., Coffey, E.L., Li, C.H., Oksuz, O., Sabari, B.R., *et al.* (2019). Mediator Condensates Localize Signaling Factors to Key Cell Identity Genes. Mol Cell *76*, 753-766 e756.

Zang, C., Schones, D.E., Zeng, C., Cui, K., Zhao, K., and Peng, W. (2009). A clustering approach for identification of enriched domains from histone modification ChIP-Seq data. Bioinformatics *25*, 1952-1958.

Zhang, Y., Liu, T., Meyer, C.A., Eeckhoute, J., Johnson, D.S., Bernstein, B.E., Nusbaum, C., Myers, R.M., Brown, M., Li, W., *et al.* (2008). Model-based analysis of ChIP-Seq (MACS). Genome Biol *9*, R137.

Zhao, D.M., Yu, S., Zhou, X., Haring, J.S., Held, W., Badovinac, V.P., Harty, J.T., and Xue, H.H. (2010). Constitutive activation of Wnt signaling favors generation of memory CD8 T cells. J Immunol *184*, 1191-1199.

Zhao, X., Shan, Q., and Xue, H.H. (2021). TCF1 in T cell immunity: a broadened frontier. Nat Rev Immunol.

Zhao, X., Shao, P., Gai, K., Li, F., Shan, Q., and Xue, H.H. (2020). beta-catenin and gamma-catenin are dispensable for T lymphocytes and AML leukemic stem cells. Elife *9*.

Zhou, X., Yu, S., Zhao, D.M., Harty, J.T., Badovinac, V.P., and Xue, H.H. (2010). Differentiation and persistence of memory CD8(+) T cells depend on T cell factor 1. Immunity *33*, 229-240.

Shan and Zhu et al. Figure 1

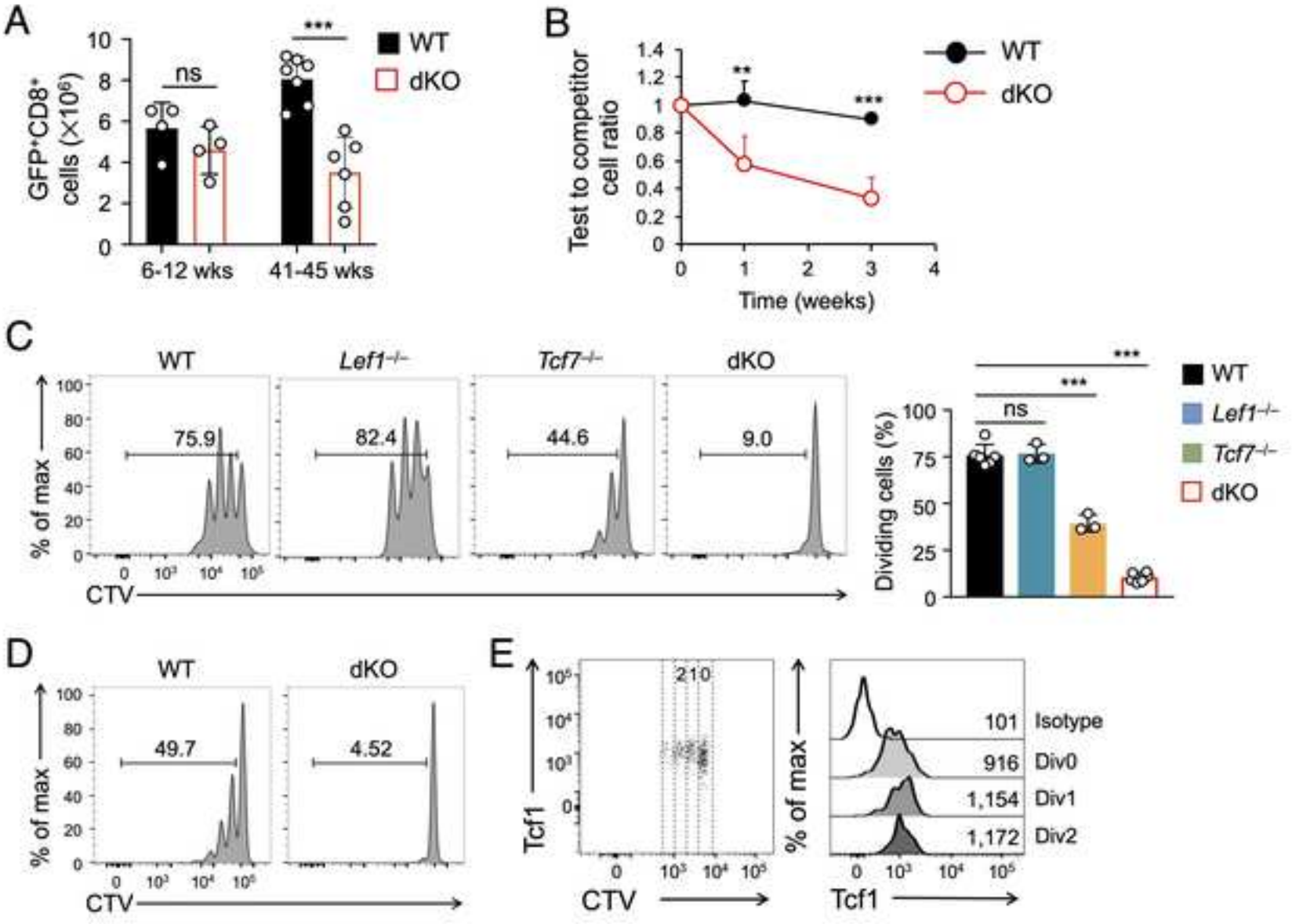

Shan and Zhu et al. Figure 2

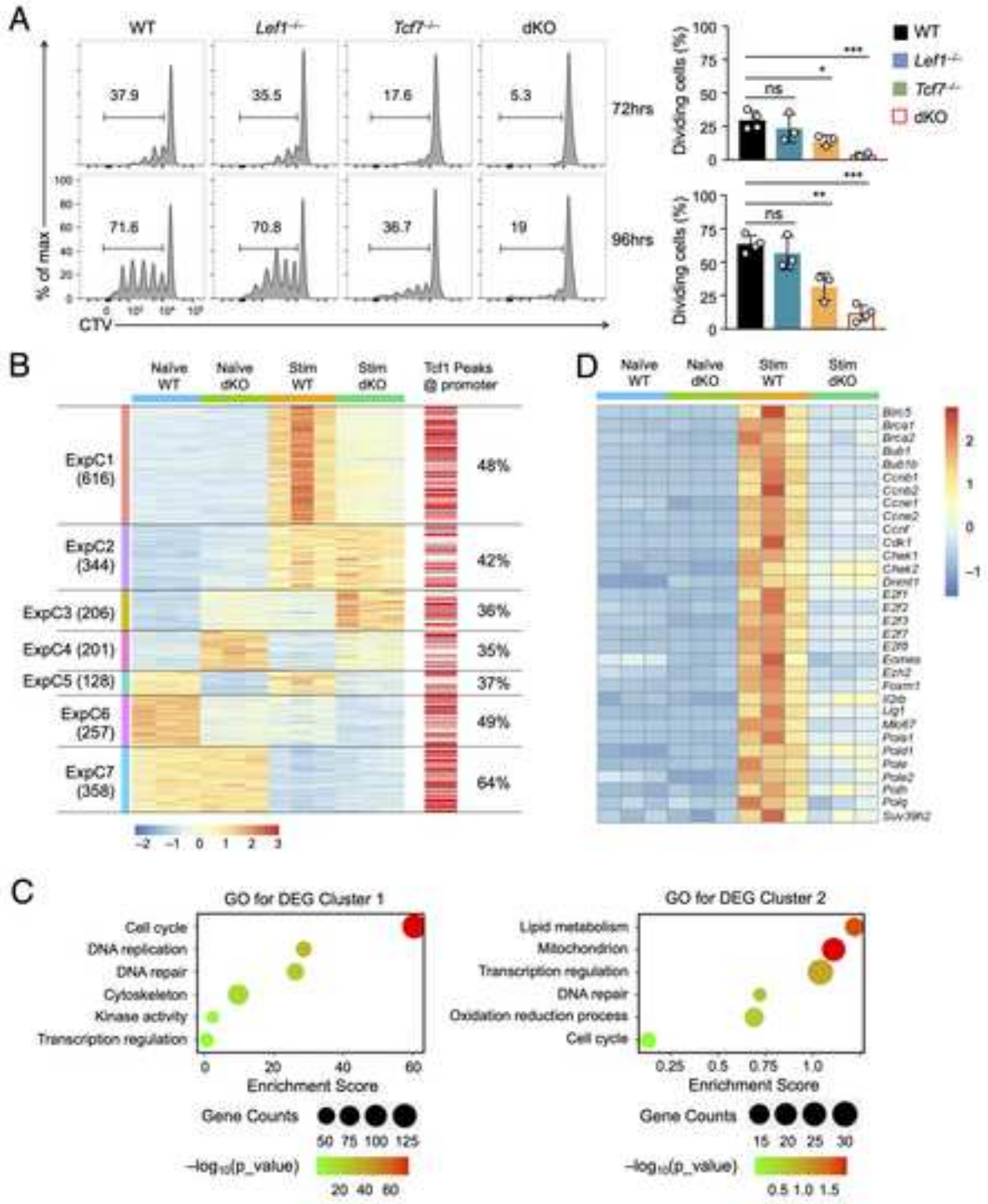

Shan and Zhu et al. Figure 3

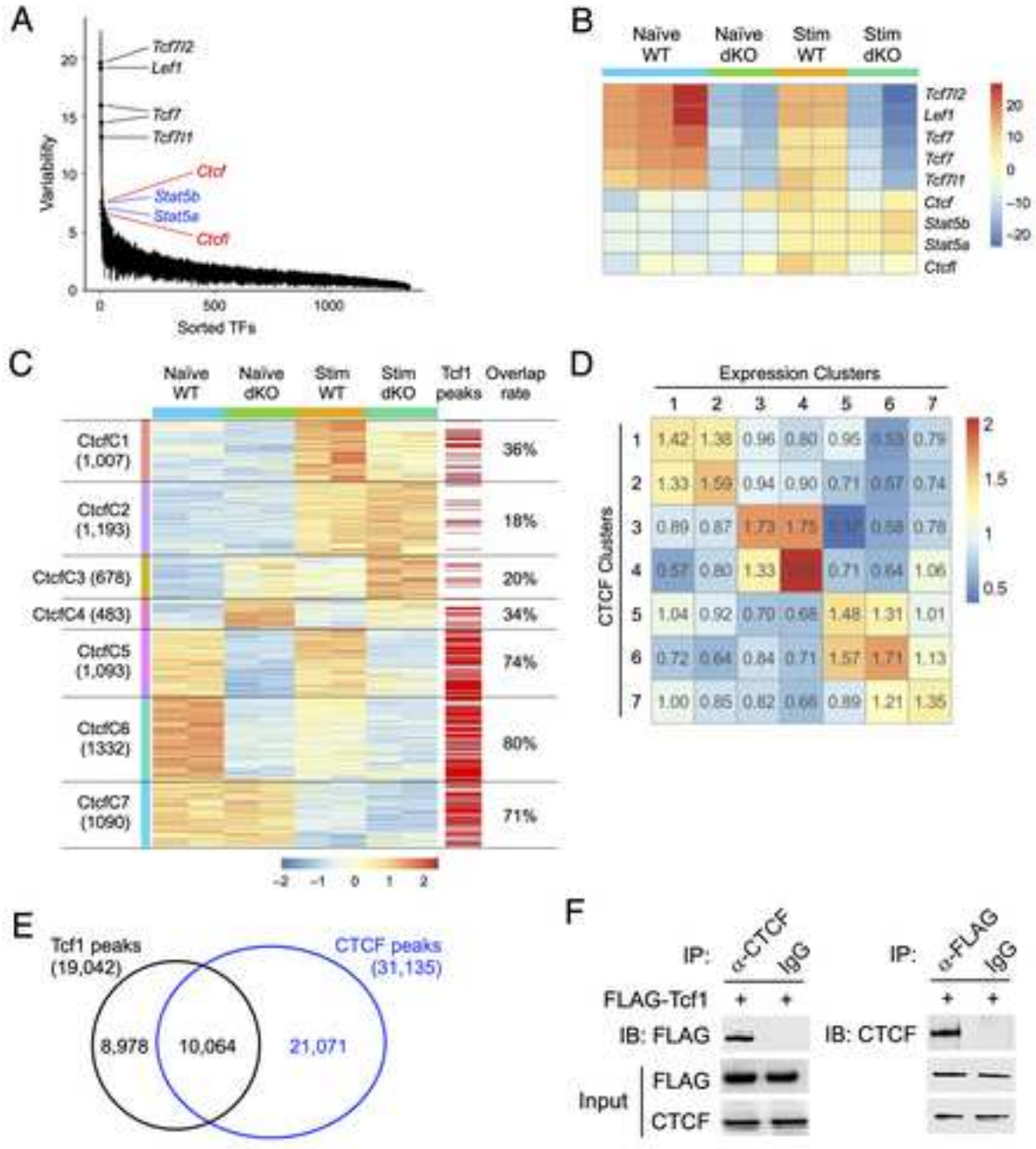

Figure 4

Click here to access/download;Figure;Shan Figure 4.jpg

Shan and Zhu et al. Figure 4

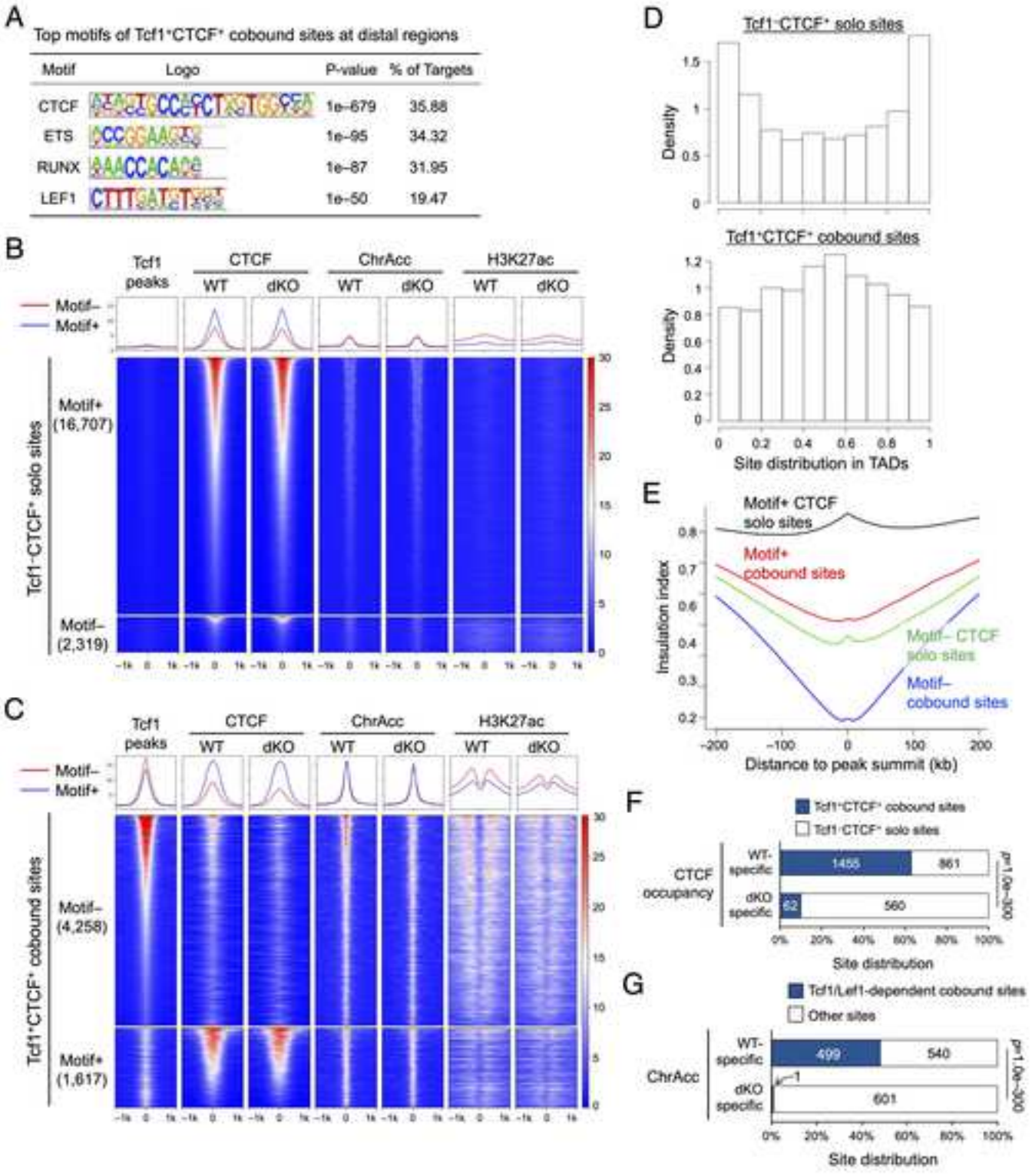

Shan and Zhu et al. Figure 5

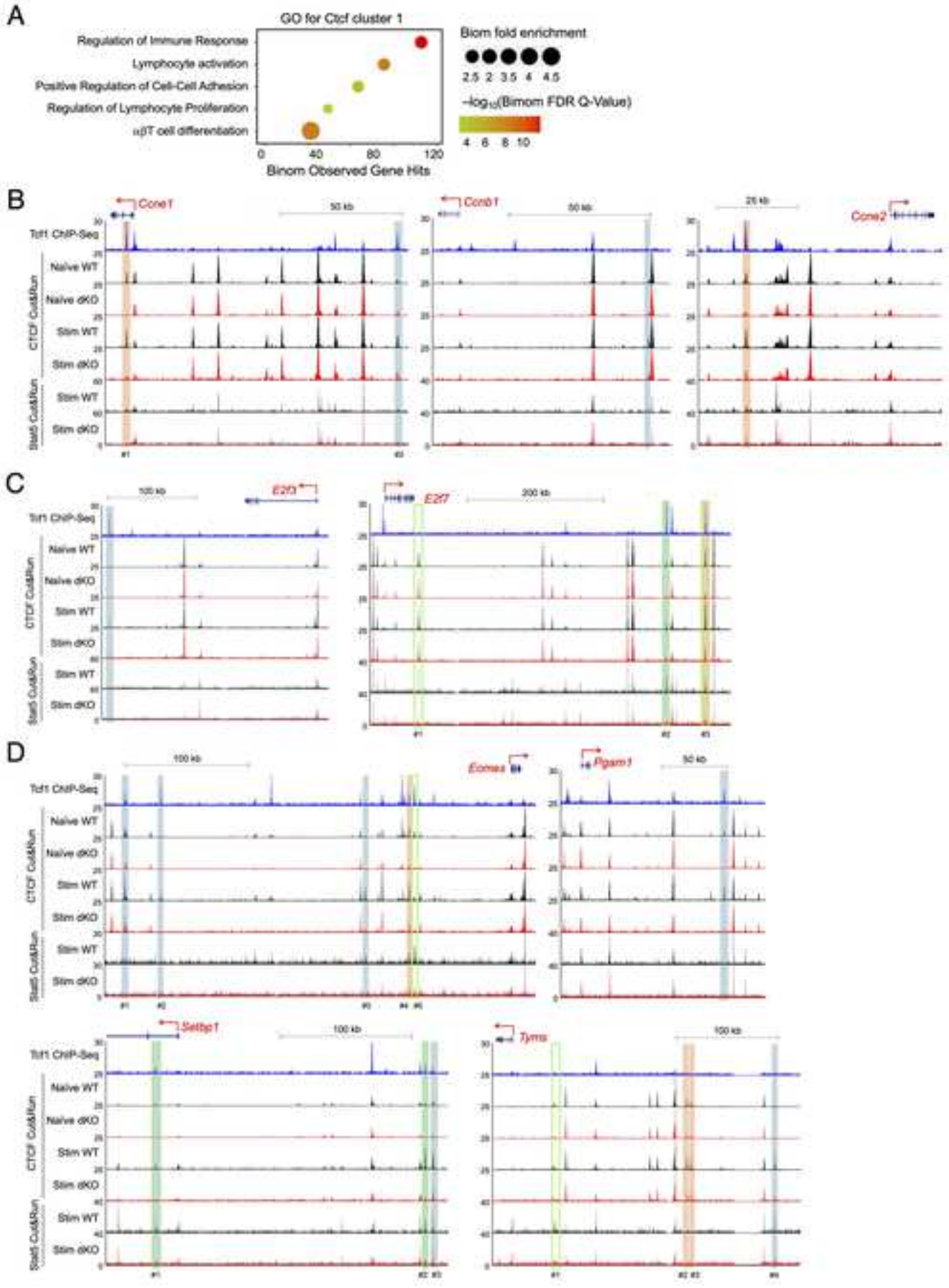

Figure 6

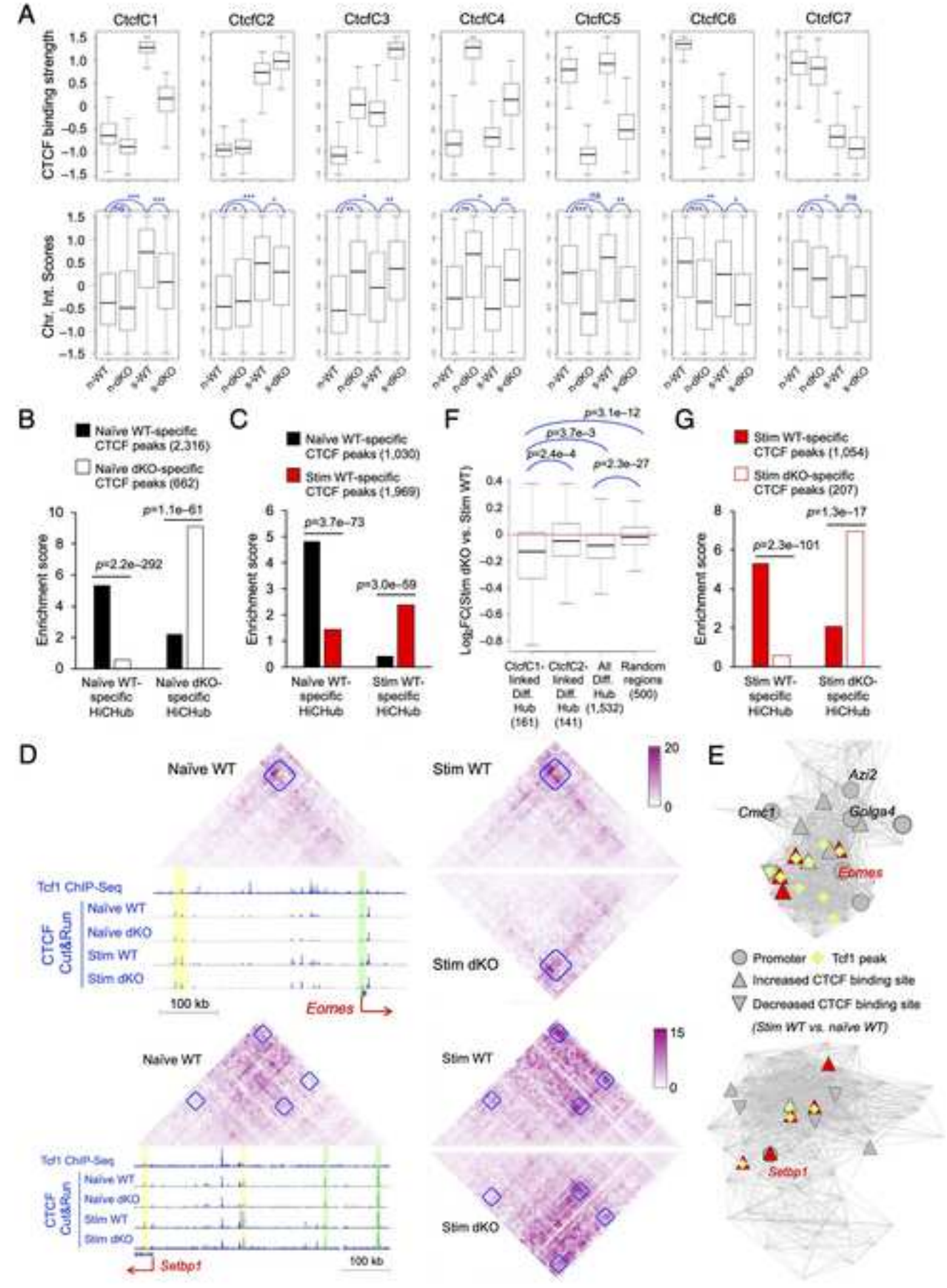

Shan and Zhu et al. Figure 7

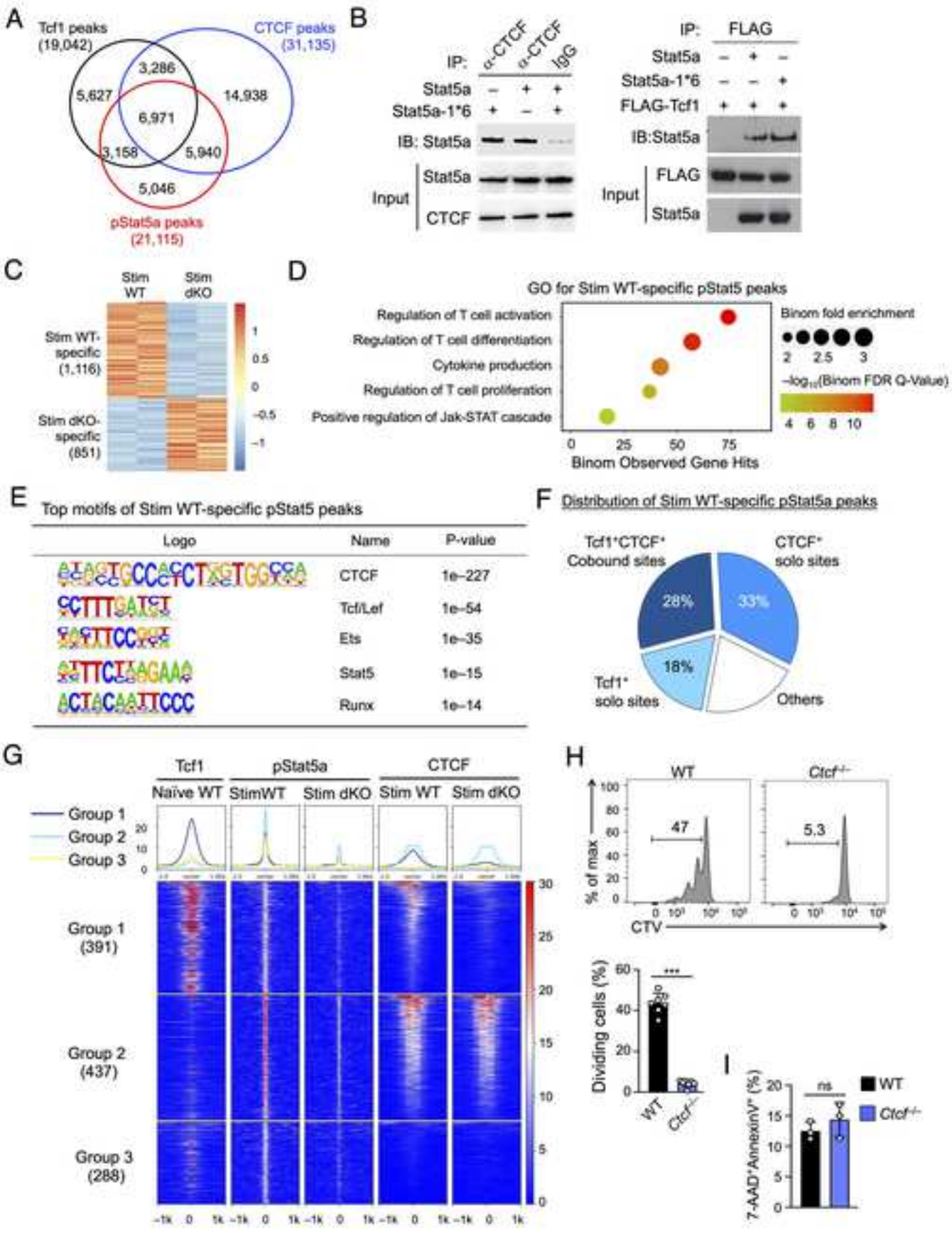

Shan and Zhu et al. Figure S1

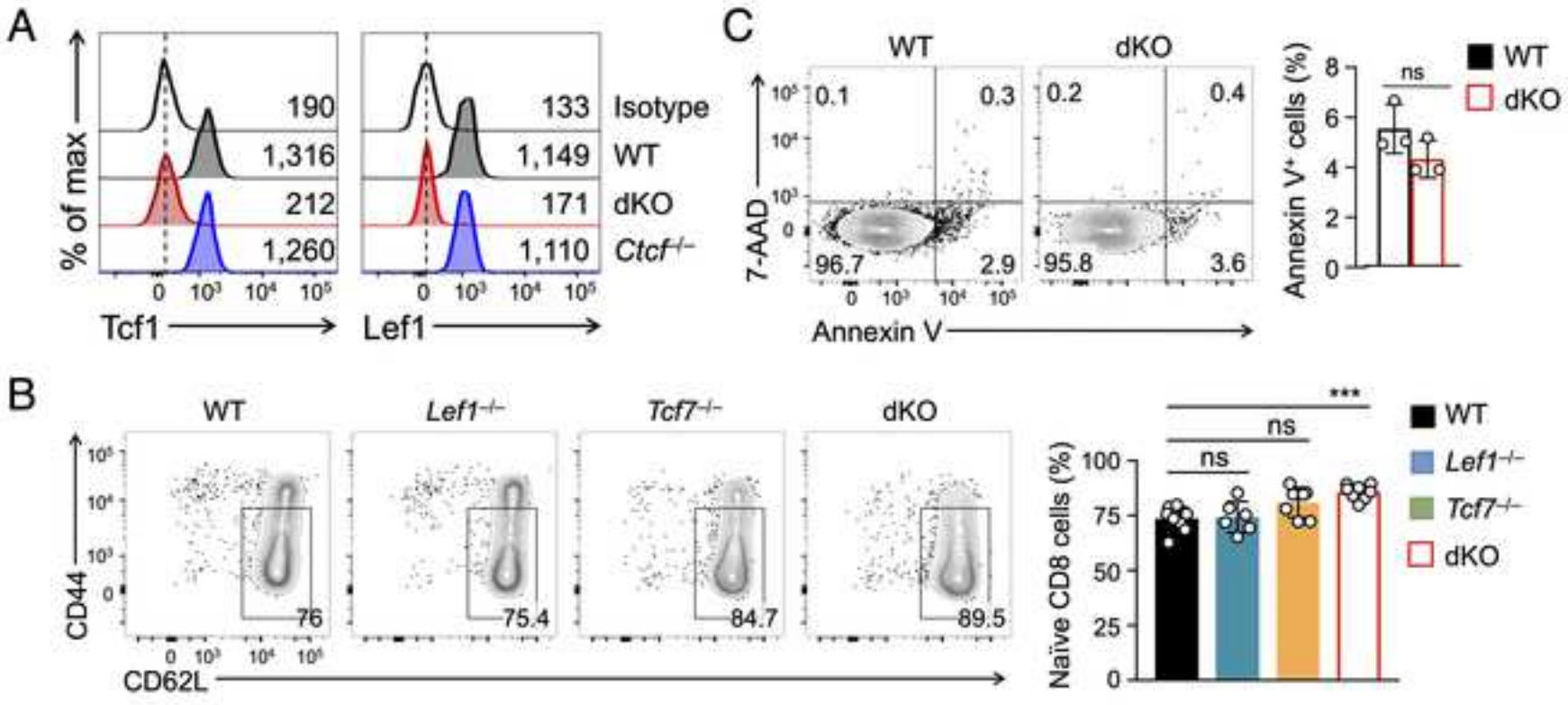

Shan et al. Figure S2

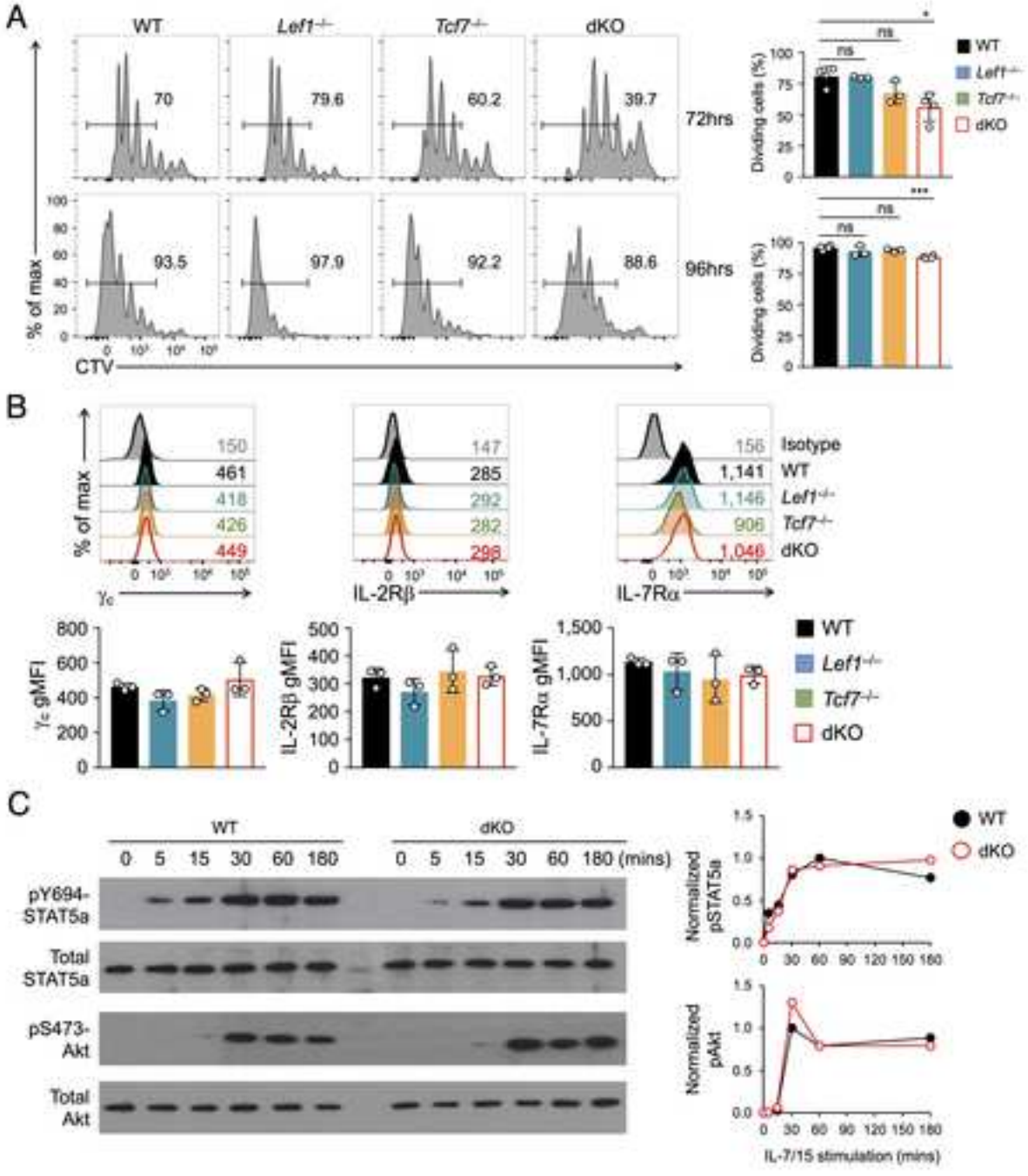

Supplemental Figure 3

Click here to access/download;Supplemental Text and Figures;Shan Figure S3.jpg

Shan et al. Figure S3

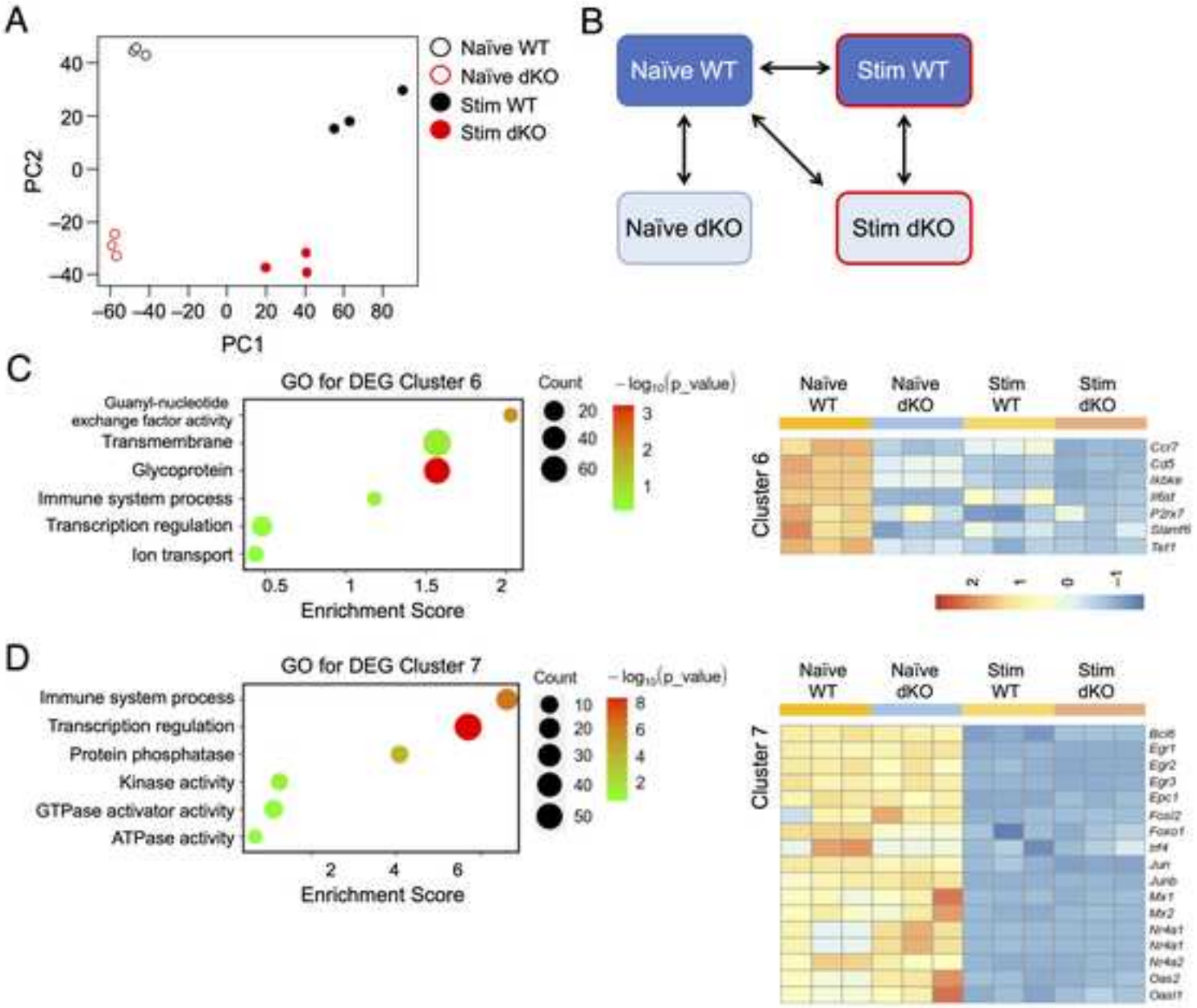

Shan and Zhu et al. Figure S4

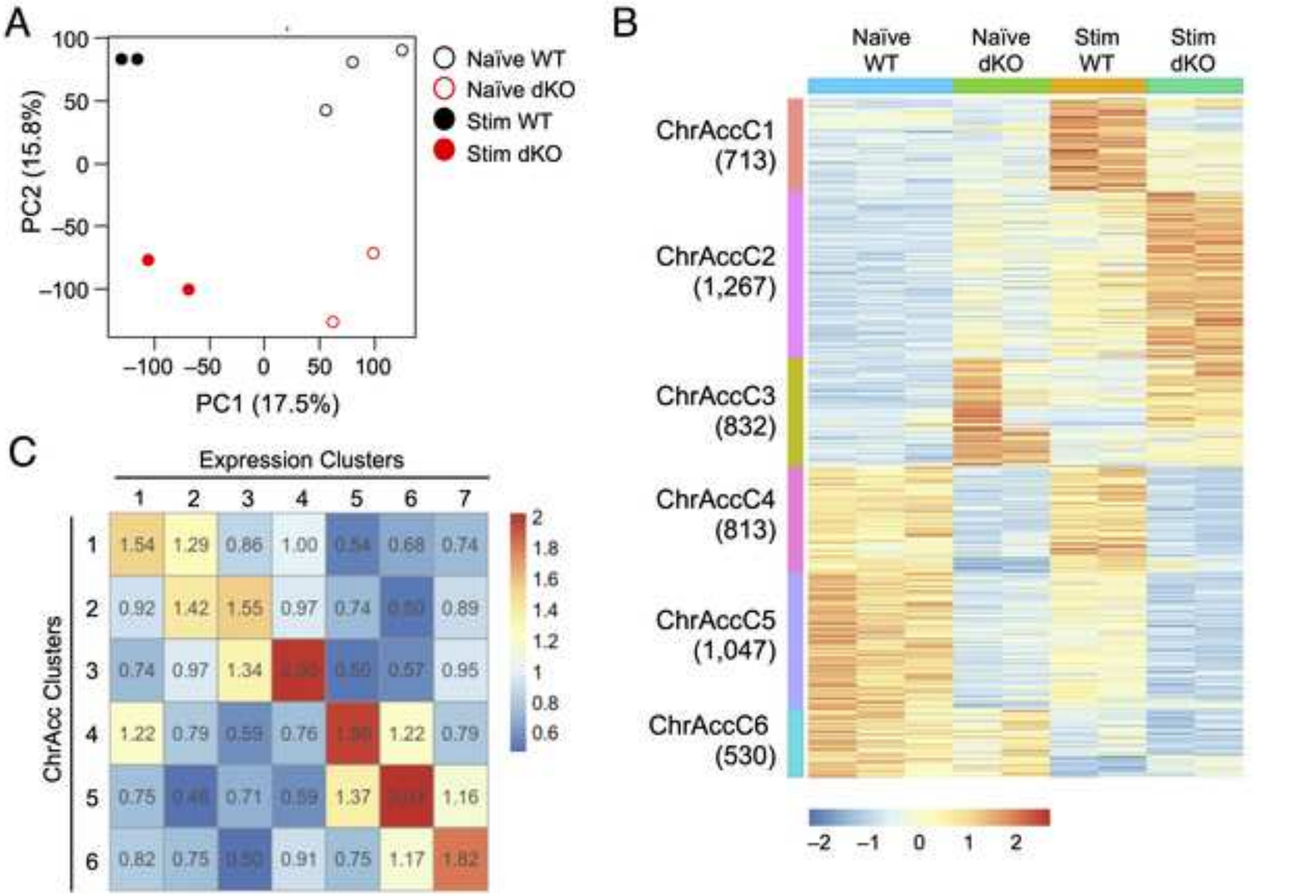

Shan and Zhu et al. Figure S5

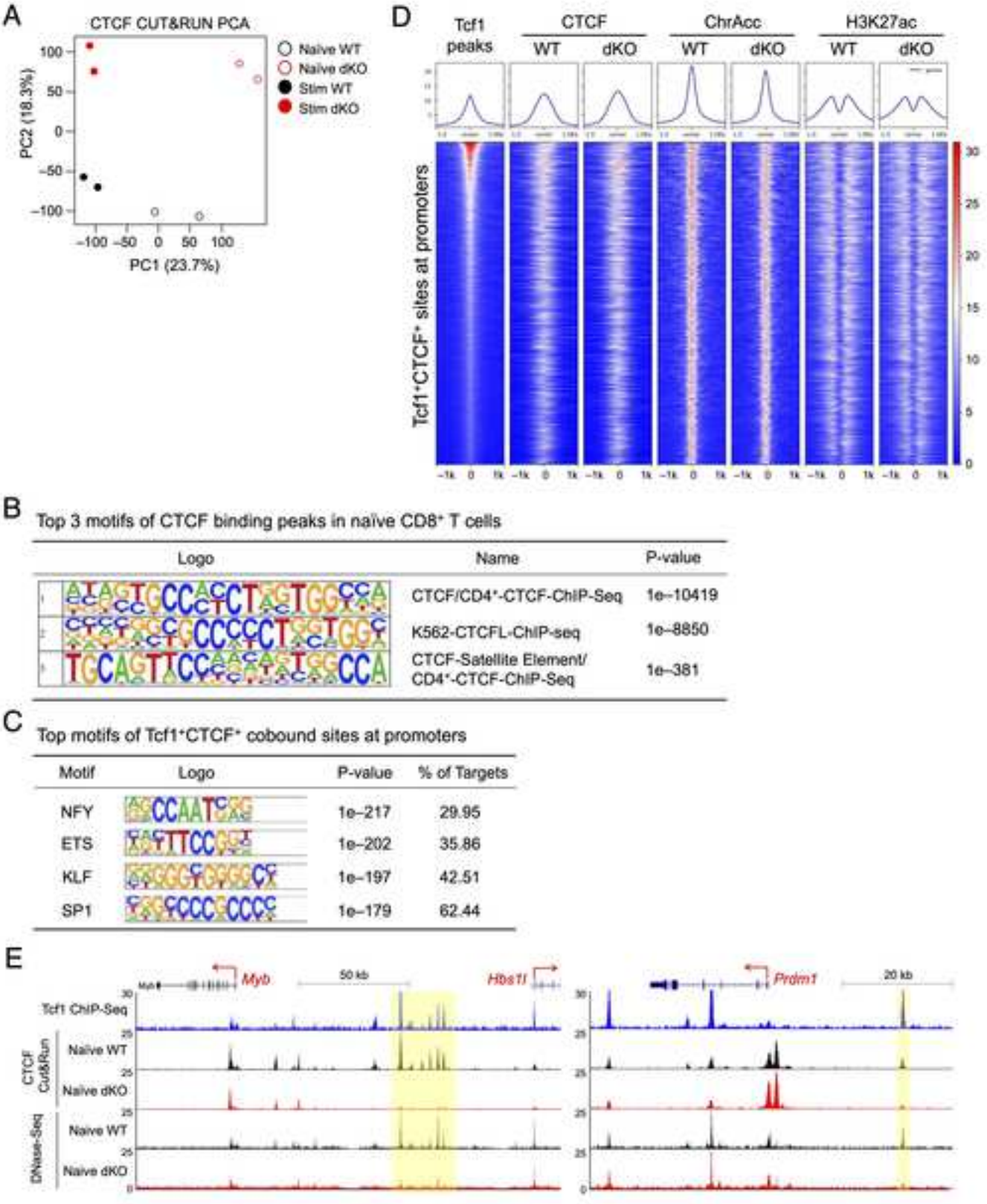

Supplemental Figure 6

Click here to access/download;Supplemental Text and Figures;Shan Figure S6.jpg

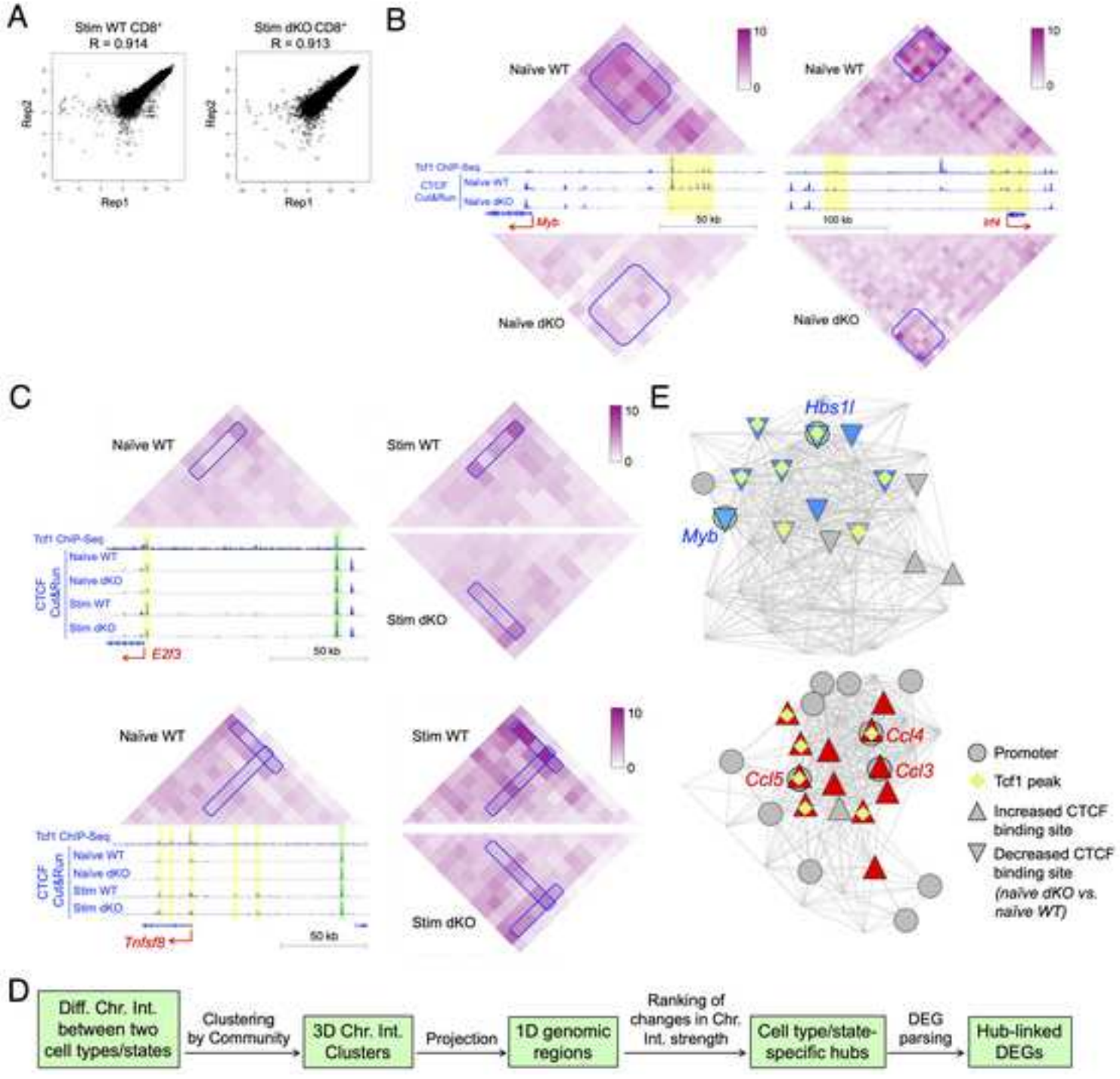

Shan and Zhu et al. Figure S7